ISSN 8755-6839

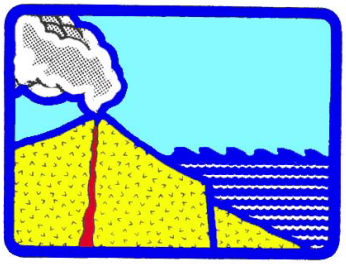

SCIENCE OF TSUNAMI HAZARDS

The International Journal of The Tsunami Society

Volume 23 Number 1 Published Electronically 2005

TSUNAMI RELICS ON THE COASTAL LANDSCAPE WEST OF LISBON, PORTUGAL 3

Anja Scheffers and Dieter Kelletat
University of Duisburg-Essen
Essen, Germany

CRITICAL EVALUATION FOR THE STATE OF HAWAII SUBSEQUENT TO THE 26 DECEMBER 2004 ASIAN TSUNAMI 17

Daniel A. Walker
Tsunami Memorial Institute
Haleiwa, Hawaii, USA

THE EARTHQUAKE AND TSUNAMI OF NOVEMBER 21, 2004 AT LES SAINTES, GUADELOUPE, LESSER ANTILLES 25

Narcisse Zahibo, Efim Pelinovsky, Emile Okal, Ahmet Yalciner, Christian Kharif, Tatiana Talipova, and Andrey Kozelkov

Pointe-a-Pitre, France; Nizhny Novgorod, Russia; Evanston, USA; Ankara, Turkey; Marseille, France; Nizhny Novgorod, Russia

NUMERICAL MODELING OF THE GLOBAL TSUNAMI: INDONESIAN TSUNAMI OF 26 DECEMBER 2004 40

Zygmunt Kowalik
Institute of Marine Science, University of Alaska, Fairbanks, USA
Tom Logan
Arctic Region Supercomputing Center, Fairbanks, AK, USA
Willliam Knight and Paul Whitmore
NOAA/NWS/WCATWC, Palmer, AK, USA

OBJECTIVE: **The Tsunami Society** publishes this journal to increase and disseminate knowledge about tsunamis and their hazards.

DISCLAIMER: Although these articles have been technically reviewed by peers, **The Tsunami Society** is not responsible for the veracity of any statement, opinion or consequences.

Submit manuscripts of articles, notes or letters to the Editor. If an article is accepted for publication the author(s) must submit a scan ready manuscript, a TeX or a PDF file in the journal format. Issues of the journal are published electronically in PDF format. Recent journal issues are available at

http://www.sthjournal.org.

Tsunami Society members will be advised by e-mail when a new issue is available. There are no page charges or reprints for authors.

Issues of the journal from 1982 thru 2004 are available in PDF format at

http://epubs.lanl.gov/tsunami/

and on a CD-ROM from the Society to Tsunami Society members.

ISSN 8755-6839 **http://www.sthjournal.org**

Published Electronically by The Tsunami Society in Honolulu, Hawaii, USA

TSUNAMI RELICS ON THE COASTAL LANDSCAPE WEST OF LISBON, PORTUGAL

Anja Scheffers
Dieter Kelletat

Department of Geography – Geomorphology and Quaternary Research
University of Duisburg-Essen
Universitätsstr. 15
D-45141 Essen, Germany

e-mail: anja.scheffers@uni-essen.de

ABSTRACT

Lisbon and the mouth of the river Tagus (Tejo) are known to have suffered from the great earthquake and tsunami of November 1st, 1755. Whereas historical sources mention tsunami waves and describe inundation in Lisbon, field evidence from this event has been found only along the Algarve coast and the Spanish Atlantic coast in the south. Our observations in the Cabo da Roca-Cascais area west of Lisbon resulted in the discovery of several very significant tsunami relics in the form of single large boulders, boulder ridges, pebbles and shells high above the modern storm level. Deposition of large amounts of sand by the tsunami waves has intensified eolian rock sculpturing. Abrasion of soil and vegetation still visible in the landscape may point to the great Lisbon event of only some 250 years ago, but radiocarbon and ESR datings also yielded older data. Therefore, we have evidence that the Portuguese coastline has suffered more than one strong tsunami in the Younger Holocene.

Science of Tsunami Hazards, Vol. 23, No. 1, page 3 (2005)

1. INTRODUCTION

On November 1st, 1755, an earthquake with a magnitude of 8.5 to 8.9 on the Richter scale occurred several hundred kilometers southwest of Lisbon near the Gorringe Bank, where the European and African plates move along each other. It was one of the greatest disasters in human history.The number of casualties caused by the tsunami triggered by the earthquake has been estimated to be about 900, whereas the total number of fatalities was near 60,000. According to 130 historical sources, recently checked again by Baptista *et al.* (1998), run-up values were more than 15 m near Cabo Sao Vicente and at Cadiz, and in Lisbon itself inundation reached at least 250 m. Geomorphologic and sedimentologic proofs of a strong tsunami impact have been detected along the Algarve coast in southern Portugal by Andrade (1992), Dawson *et al.* (1995), and Hindson & Andrade (1999), mostly as washover fans in coastal barriers. Luque *et al.* (2001) were able to identify sand sheets and pebbles dislocated more than two thousand years ago along the barrier coastline of southern Spain, deriving from a tsunami with wave energies and run-up heights similar to or only a little less than those of the year 1755. Field surveys at Cabo de Trafalgar in southern Atlantic Spain by Whelan & Kelletat (2003) resulted in the mapping of large boulders of up to 100 tons in the intertidal area, and smaller boulders and shelly sands thrown over the cape with run-ups of at least +19 m asl. Astonishingly, to date no field inspection has been undertaken in the vicinity of Lisbon itself, although the coastal section north of the Tagus river mouth from Cascais to Cabo da Roca (see Fig. 1) has been extremely exposed to all tsunami waves from the Gorringe area in the SW. The reason may be that this coastline is a rocky one with medium to steep slopes from about +10 to +20 m asl extending into the sea, or even vertical cliffs of up to more than 30 m in height. Deposits of tsunami waves along this type of coastline are not to be expected; geologists and sedimentologists prefer to inspect accumulative geomorphologic units with a good stratigraphy for dating. Field research on Cyprus (Kelletat & Schellmann, 2001, 2002) and Mallorca (Bartel & Kelletat, 2003) has shown, however, that rocky shorelines may well preserve the imprints of tsunami waves.

2. FIELD OBSERVATIONS

In May 2004, the authors conducted field research in the Cascais-Cabo da Roca area west of Lisbon in order to study the fine sculpturing by shifting sands on the limestone rocks. Being aware of boulder deposits from Holocene tsunami in other regions (Mediterranean, Caribbean), we also looked for geomorphologic or sedimentologic evidence of a possible tsunami imprint from the 1755 Lisbon event in this area. As we will briefly describe below, there are several tsunami relics which may yield some good indication of run-up values and impact times.

Fig. 1 shows the study area in more detail: The broad promontory of Cabo Raso consists of gently folded limestone, forming a rocky shoreline with low cliffs and numerous deep and narrow incisions along fault lines or abraded mylonitic rocks. The rocks normally are bare of vegetation up to about 7-8 m asl because of the strong exposure to Atlantic storm waves and swell. The highest storm-moved boulders can be found at about +5.5 m asl with a maximum of +7 m weighing nearly 100 kg in fissures. On higher ground, soil and vegetation appear, mostly on a sandy stratum of up to several meters in

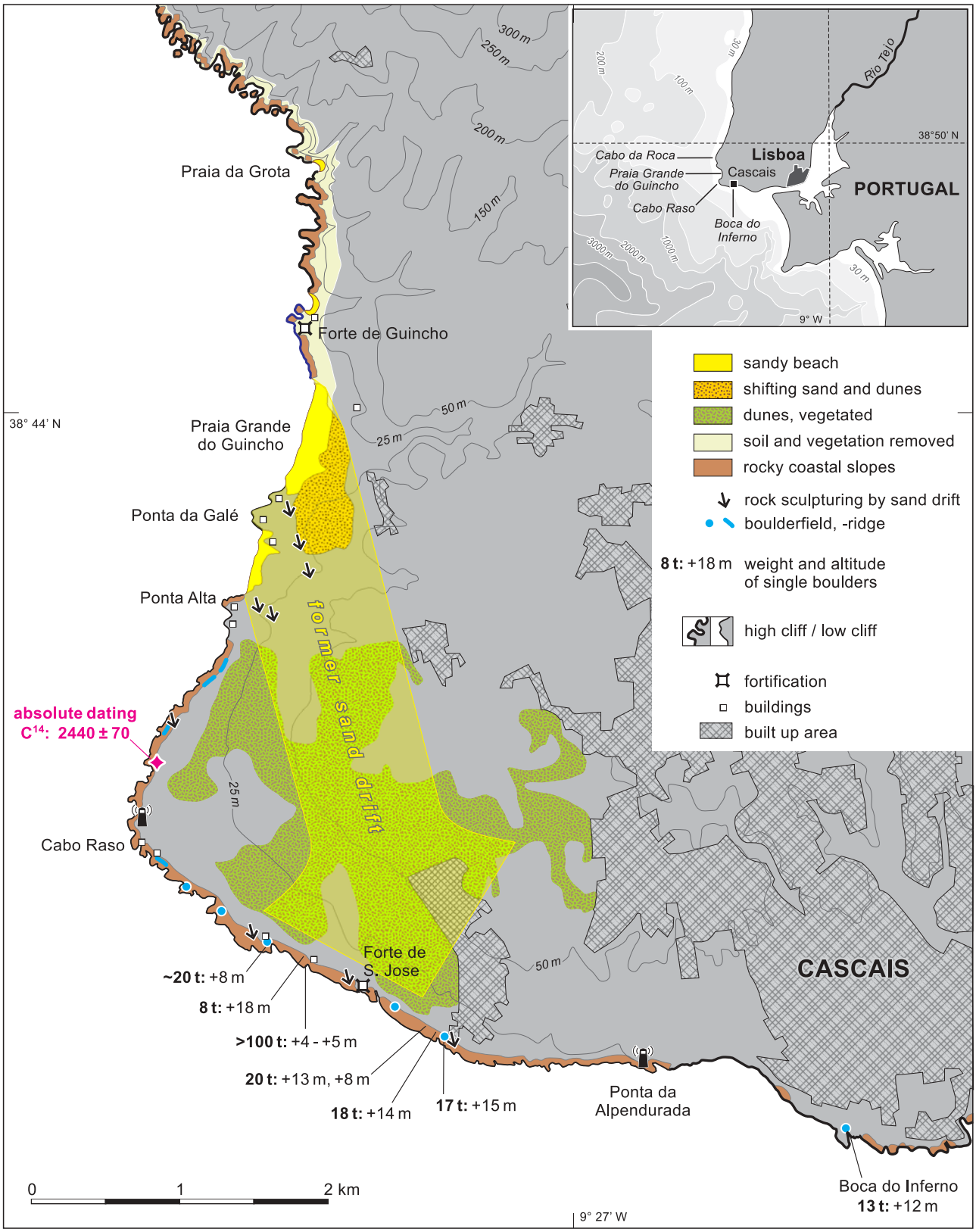

Fig. 1: Coastal features along the section Cascais-Cabo da Roca west of Lisbon.

thickness. To the east (i.e. direction of Lisbon, up the river Tagus), the coastal cliffs become higher and very steep and are strewn with huge cube-like boulders at their base, some of them exceeding 1000 tons. These giant boulders give the impression of a sudden collapse of the vertical cliffs.

More than 1 km north of Cabo Raso, sandy beaches occur with a width of about 1 km, interrupted by the small promontory of Ponte da Galé. Evidently sand supply to these beaches is very good, as can be seen by the development of a foredune belt as well as high and bare sand dunes which are shifting inland. During stronger northerly winds, shifting sand is a danger to road traffic in this area. The sand is rather fine (about 0.05 mm in diameter), highly polished and rounded and shows 3-5% percent carbonate particles from broken shells. North of Guincho beach, the deeply incised rocky shoreline becomes steeper and higher, containing some small pocket beaches on the west-facing section. Closer to Cabo da Roca, cliffs of far more than 100 m occur, cut into cristalline rocks and strongly folded and faulted sedimentary units, disturbed by dikes, the whole being a very complicated geologic situation.

As is normal along limestone coasts, a belt of bio-erosive rock pools with a characteristic sharp miniature relief has developed along the surf line on the limestone reaching a height of about +4 to 5 m asl. Higher up, the bare carbonate rocks exhibit smoother contours typical of karst solution under a soil cover. The intensity of the karstification can be seen from numerous perpendicular solution shafts many meters deep. From about +8 to 9 m asl, these hollows are more or less filled with relics of an old red soil with caliche, belonging to this phase of deep karstification in Pleistocene times. The red Pleistocene soil is mostly covered by a sandy stratum containing a dark brown soil from Holocene times (up to at least 2 m deep, B-horizons preserved), which itself may be covered by younger sands with only a very light brown colouring, thus showing a very young and short soil development (Fig. 2). Traffic and tourist impact have destroyed these soils in many areas of the coast. Further inland, dense shrubs and pine forests cover extended sand bodies, partly showing dune features now fixed by vegetation.

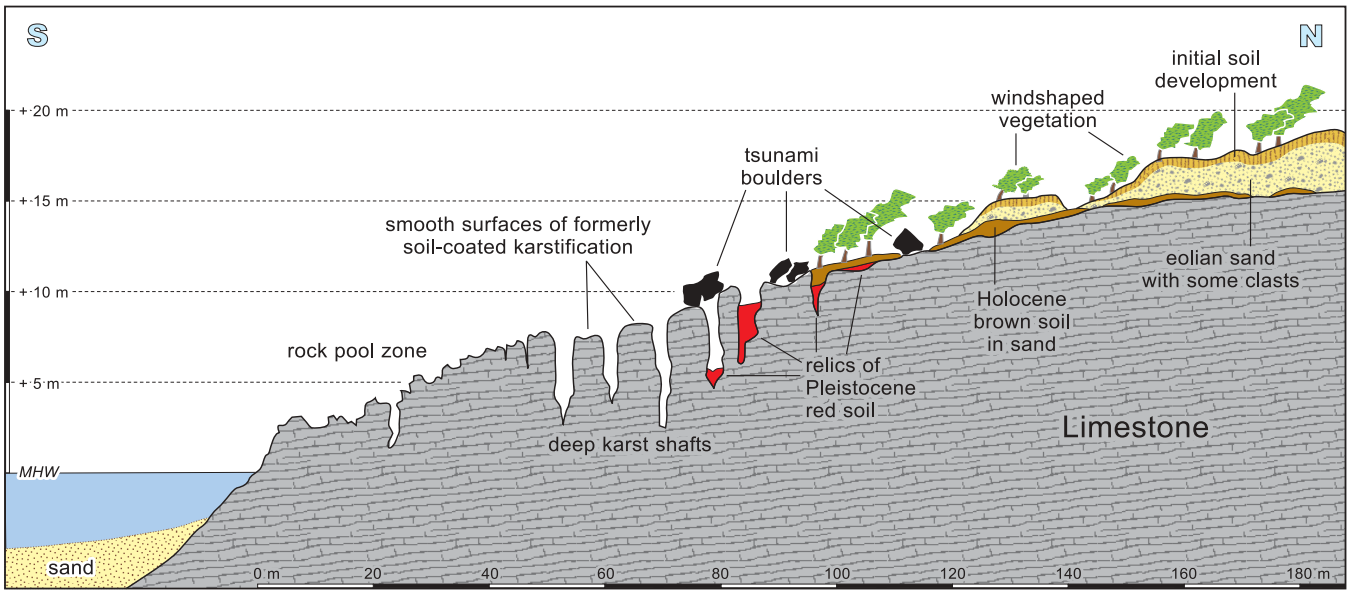

Fig. 2: Schematic cross-section of the rocky shoreline in the Cabo Raso area.

Outside the reach of even the strongest storm waves – as is visible from the soil and vegetation as well as the weathering on rocks –, single boulders have been deposited on the boundary of or even within the denser vegetation. Some distinctive boulders have been mapped in Fig.1. Weights ranging from more than 10 tons to about 20 tons can be found up to nearly +20 m asl (Figs. 3-5), and, 500 m west of the Forte de José, a boulder of more than 100 tons (longest axis 8 m) has been dislocated at +4 to 5 m asl (Fig. 6). On the south facing shoreline as well as on the westerly exposure north of Cabo Raso, smaller boulder fields (more than 50 fragments) or boulder ridges occur, again at around +10m or higher (Figs. 7 and 8).

Single boulders are not only dislocated for 50 m or more against gravity on a rough surface, but turned upside down, as can be seen from smooth karst forms at their bases. The status of their weathering, including karstification, soil development around them as well as pioneer vegetation on these boulders, points to the fact that over many decades or even centuries they have not been moved, which excludes strong storm impacts. Observations along stormy coastlines of the world as well as the state of the art of the knowledge of coastal boulder movement by waves (Nott, 1997, 2003; Scheffers, 2002, 2003, 2004) show that there is only one force which can move boulders of this size high above the surf line, namely tsunami waves. Therefore, we can take these boulders as being proof of one or more tsunami events along this coastal section of Portugal.

This conclusion is confirmed by the presence of well-rounded sand with pebbles (at some places enriched by deflation) and shells, both around the boulder deposits and higher and further inland. North of Praia Grande do Guincho, the size of the dislocated boulders is less than that of those in the south, reaching several tons landward of Forte de Guincho, which is located at +12 m asl. At around +30 m asl, the boulders weigh only 50-300 kg and are mixed with shelly sand and extremely well-rounded quartz pebbles of a smaller size (see also Fig. 9).The petrography of these boulders shows granite, quarzite, diabase, basalt, sandstone, limestone, and others. As

Fig. 3:
Tsunami boulder of about 20 tons, turned upside down at +10 m east of Cabo Raso.

Fig. 4:
Tsunami boulder of 25 tons near Forte de San José, moved inland for at least 30 m.

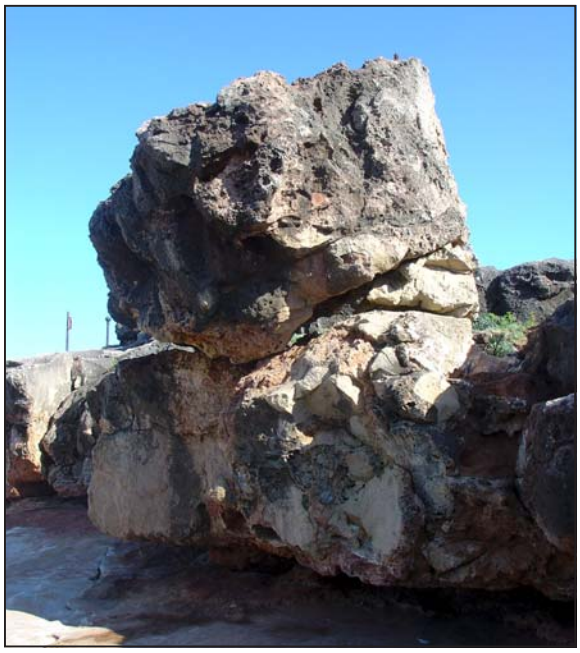

Fig. 5:
Tsunami boulder of more than 12 tons in a precarious setting at +13 m asl at Boca do Inferno, Cascais.

Fig. 6:
The largest tsunami boulder, broken by dislocationof several meters upwards into 4 pieces at +4-5 m asl about 400 m west of Forte de San José (Cascais). When first moved, the boulder had a weight of nearly 200 tons. The largest fragment with a longitudinal axis of about 8 m, still weighs more than 100 tons.

Fig. 7:
Tsunami boulder ridge with imbrication east of Cabo Raso at about +12 m asl.

Fig. 8:
Tsunami boulder field at about +14 m asl north of Cabo Raso.

Fig. 9:
Tsunami deposits (basaltic pebbles, coarse sand, shell fragments north of Guincho beach at +35 m asl.

mapped in Fig. 1, a rather sharp line separates dense shrubby vegetation from nearly bare land seaward of it, exhibiting an abrasive cutting of vegetation and soil in younger historical times. In some places, this line reaches +50 m asl, and beach pebbles and sand can be found even higher up. Some now vegetated dune-like sand bodies contain well-rounded floating boulders, and in total, these features are evidence of a tsunami with run-up heights of more than +50 m locally in this area.

What needs to be explained is the huge amount of sand and dune-like features which are bare or under vegetation from the town of Cascais to the Cabo Raso promontory. Two sources may be responsible for this: One is Guincho beach in the north, which in fact delivers shifting sands from direction NNW or 345° far inland, the other may be tsunami waves taking fine sediments from the open mouth of the Tagus with waves from SW. Evidence of the latter assertion are the large dislocated boulders close to the shoreline and the floating boulders and clasts within the sandy deposits inland. The sand directly east of Cabo Raso is much coarser than that of Guincho beach, with a diameter of around 1mm, bad sorting, less carbonate content and less polished grains than sand from the Tagus.

Shifting sands from Guincho beach have formed fine sculptures which are elongated and strictly parallel to 345° on bare rock (see arrows in Fig. 1 and Fig. 10). Through wind sculpting, the karst topography has been transformed into asymmetric rock outcrops (Fig. 11). Similar ones can be seen along the south-facing shorelines east of Cabo Raso (Figs. 12 and 13), evidently formed by wind from 345°, but now inactive with a slight destruction of the wind-polished surfaces by karstification in the range of several millimeters to 1 cm. These forms are evidence of a strong sand shift from the Guincho area across the broad promontory and from land to sea along its south shore. It is certainly not necessary to discuss climatic changes during more recent historical times to explain drifting sand in this landscape, because this might have also been caused by deforestation (cutting or burning). We are convinced, however, that the phase of sand sculpting on the south coast from direction 345° was triggered by sand from the Guincho area, where tsunami waves have picked up huge amounts of fine particles from the shallow foreshore.

Fig. 10:
Sculpturing of limestone rock shaped by modern sand drift south of the Guincho beach.

Fig. 11:
Rock outcrops of limestone have been sculpted asymmetrically by sand polishing south of Guincho beach.

Subsequently, the sand was shifted by strong northerly winds across the promontory to the south coast. By this process, some of the grains were broken and, after deposition, the carbonate content nearly disappeared, and a light brownish soil developed on the dune-like deposits. After the dislocation of this huge mass of sand to the south, the normal sand supply of today (which is still rather strong) has been overwhelmed by vegetation after several hundred meters of movement, and the southward sand transport into the Tagus ceased.

In sum, we found several evidences of tsunami in this area:

- boulders too large for transportation by storm waves dislocated high above the surf and far inland,
- boulder fields and boulder ridges with delicate setting and imbrication,
- floating boulders and clasts within chaotic sand deposits, i.e. typical bimodal tsunami sediments,
- beach sand and perfectly rounded beach pebbles and boulders far inland and up to more than +50 m asl,
- abrasion of soil and vegetation with a sharp scar, best identifiable on aerial photographs taken north of Guincho beach (for position compare Fig. 1),
- huge amounts of sand deposited in one short pulse, subsequently transported inland and seaward to the south,
- shells and molluscs of different species incorporated into the finer deposits high above sea level.

As concerns the boulder tracks, imbrication, the deposition of the largest boulders and vegetation scars, the direction of the tsunami undeniably came from SW to SSW. Run-up heights along the south-facing shorelines were at least +20 m, because large boulders can be found at up to +18 m and, north of Guincho beach, run-up was more than +50m in places, as can be identified by the vegetation scar crossing the 50 m isohyps in Fig. 1. As regards the number of tsunami waves, we were unable to find any definite evidence in the field.

Fig. 12:
Asymmetrical wind sculpted rock outcrops on the south coast of the Cabo Raso promontory, subsequently weathered.

Fig. 13:
Although transformed by karstification, inactive rock sculptures produced by wind polishing can still be identified east of Cabo Raso. Wind direction was from left in the picture.

3. RELATIVE AND ABSOLUTE DATING

From the field survey, we have derived some inductive and objective criteria for a relative dating of tsunami in the Cascais-Cabo da Roca area:

- *first*: the position of tsunami boulders in vegetated areas and those embedded in a soil on sand many decades to several hundred years old and far beyond the reach of the modern energetic surf;
- *second*: the weathering status, including the karstification of the boulder surfaces, again several hundred years or more in age;
- *third*: the slight destruction of sand-polished surfaces on limestone outcrops by karstification within the range of a few millimeters to about one centimeter, which again may need several hundred years to form;

- *fourth*: the good development of rock pools above the surf line without any traces of destruction by tsunami waves, demonstrating that the period after this event was long enough for good bio-erosive rock-pool formation;
- *fifth*: a still visible scar along the shrubby vegetation between about +20 to +50 m asl north of Guincho beach, evidence of a destructive impact more recent than the oldest juniper and mastix bushland on the coastal slopes;
- *sixth*: the existence of coastal fortifications (Forte de Guincho in the north, Forte de San Jose in the south from 1796), i.e. about 200 years old, founded in the tsunami-affected area but not harmed by a tsunami;
- *seventh*: the good preservation of molluscs in the finer tsunami deposits.

Whereas the founding period of the fortifications may yield only an absolute minimum date of a strong tsunami impact on the Cabo Raso area of more than 200 years ago, absolute dating by radiocarbon and ESR methods on marine carbonates (*Patella* sp., *Dolium* (Tonna) *galea*) are fairly reliable indicators of the time of the tsunami events occurring along this coastline of western Portugal. The most abundant molluscs dislocated and deposited high above the surf environment are limpets (*Patella* sp., see Fig. 14). The reason may be that these gastropods are widespread on rocky coasts with no beaches, where they resist even extreme surf beat. Evidently, the tsunami waves have pulled them from their original habitats, perhaps partly by abrading the highest parts of the shells and thus producing ringlike segments as shown in Fig. 14.

As with 1755 a rather young age for radiocarbon dating (regarding the reservoir problems) is given, Prof. Dr. U. Radtke (Cologne, Germany) tested some samples with ESR technique, which was sucessfull parallel to radiocarbon with coral samples from tsunami of the Caribbean (Radtke

Fig.14:

Patella sp., extracted from tsunami sediments at +14 m north of Cabo Raso. Ringlike fragments are typical, perhaps because of abrasion of the shells' tops by tsunami waves. Radiocarbon dating yielded a conventional age of 2440+-50 BP.

et al., 2002). A sample of well preserved *Dolium* (Tonna) *galea* gave an ESR signal of some hundred years as maximum, but older than modern. This would well fit into the 18th century as does the vegetation scar north of Guincho beach. A radiocarbon datum of 2440 +-50 BP from *Patella* sp. north of Cabo Raso at +12 m asl definitely hints at an older strong tsunami impact. It is highly likely that it was the same tsunami which was identified by Luque *et al.* (2001) in southern Spain, most probably from the years 218 or 216 BC, which were mentioned in older texts. The ESR signal from this sample was the same than that of another one from north of Guincho beach at +30 m asl. They certainly are of the same age, and by this we have two sites with older historical tsunami data. One sample of Patella from south of Guincho Beach at +14 m asl gave ESR signals about 2.5 times older than those from 2440 BP, pointing to ages of Middle Holocene around 6.000 to 7.000 BP, which will well fit into the geomorphology and soil stratigraphy of the region. As a result we carefully should say that the Lisbon event of 1755 left boulders and vegetations scars up to +50 m asl and shell in the Cabo Raso-Guincho area, and that it is highly likely, that at least one older tsunami (3rd century BC) has affected this area, maybe another one at the beginning of the Holocene high sea level. Regarding the distribution of dislocated boulders, they all may have had their origin near the Gorringe Bank southwest of Cabo Sao Vicente, SW Portugal.

4. DISCUSSION AND CONCLUSIONS

The different tsunami deposits preserved north of the mouth of the Tagus west of Lisbon evidently point to a strong event with run-up values of +20 to +50 m asl, depending on coastal configurations and exposure. We did not find clear evidence of the number of tsunami waves or backwash features but at least some hints as to the minimum age of the tsunami such as weathering intensity and vegetation and soil development. This was about 200-300 years ago, thus pointing to the well-known historical catastrophe of the year 1755. Uncertainties remain concerning the intensity of soil development and the degree of karstifikation on dislocated boulders, whereas the distinctive vegetation scar north of Guincho beach certainly must have been caused within a limited time frame in order to have been preserved. Absolute dating by ESR and radiocarbon methods, however, yielded the clear result that at least two major tsunami events have impacted this coastline in historical times (i.e. 18th century and 3rd century BC). Both were of a very similar strength and had similar run-ups as well as the same direction (from SW). There is no doubt of this because of the evidence of the vegetation scar that in 1755 – triggered by the open exposure to the tsunami wave from the southwest and the steep slopes in the embayment southeast of Cabo da Roca – tsunami run-up reached heights of at least +50 m asl in places. These values are much higher than those cited to date for the Lisbon event. On the basis of our observations and findings along the short coastal section between Cascais and Cabo da Roca, we are convinced that there are many more tsunami deposits from the 1755 Lisbon event and earlier impacts to be found along the coastlines of Portugal (and southern Spain, Morocco and other areas), and that the two historical tsunami events identified and dated so far cannot have been the only strong ones in the coastal regions of the Iberian peninsula.

ACKNOWLEDGEMENTS

We thank Sander Scheffers for his assistance during field work and Prof. Dr. Ulrich Radtke (University of Cologne) for the ESR datings.

REFERENCES

Andrade, C., 1992. Tsunami generated forms in the Algarve barrier islands. Science of Tsunami Hazards 10, 21-34.

Baptista, M.A., Heitor, S., Miranda, J.M., Miranda, P., Victor, L.M., 1998. The 1755 Lisbon Tsunami; Evaluation of the Tsunami Parameters. Journal of Geodynamics, 25 (2), 143-157.

Bartel, P., Kelletat, D., 2003. Erster Nachweis holozäner Tsunami im westlichen Mittelmeergebiet (Mallorca, Spanien) mit einem Vergleich von Tsunami- und Sturmwellenwirkung auf Festgesteinsküsten. Berichte Forschungs- und Technologiezentrum Westküste; Universität Kiel, Büsum, 28, 93-107.

Dawson, A.G., Hindson, R.A., Andrade, C., Freitas, C., Parish, R., Bateman, M., 1995. Tsunami sedimentation associated with the Lisbon earthquake of 1 November AD 1755: Boca do Rio, Algarve, Portugal. The Holocene, 5 (2), 209-215.

Hindson, R.A., Andrade, C., 1999. Sedimentation and hydrodynamic processes associated with the tsunami generated by the 1755 Lisbon earthquake. Quaternary International, 56, 27-38.

Kelletat, D., Schellmann, G., 2001. Sedimentologische und geomorphologische Belege starker Tsunami-Ereignisse jung-historischer Zeitstellung im Westen und Südosten Zyperns. Essener Geographische Arbeiten, 32, 1-74.

Kelletat, D., Schellmann, G., 2002. Tsunamis on Cyprus – Field Evidences and ^{14}C Dating Results. Zeitschrift für Geomorphologie, NF, 46 (1), 19-34.

Luque, L., Lario, J., Zazo, C., Goy, J.L., Dabrio, C.J., Silva, P.G., 2001. Tsunami deposits as paleoseismic indicators: examples from the Spanish coast. Acta Geologica Hispanica, 36 (3-4), 197-211.

Luque, L., Lario, J., Silva, P.G., Zazo, G., Goy, J.L., Dabrio, C.J., 2002. Sedimentary record of a tsunami during Roman times, Bay of Cadiz, Spain. Journal of Quaternary Science, 17 (5-6), 623-631.

Nott, J., 1997. Extremely high wave deposits inside the Great Barrier Reef, Australia: determining the cause – tsunami or tropical cyclone. Marine Geology, 141, 193-207.

Nott, J., 2003. Waves, coastal boulder deposits and the importance of the pre-transport setting. Earth and Planetary Science Letters, 210, 269-276.

Radtke, U., Schellmann, G., Scheffers, A., Kelletat, D., Kromer, B., Kasper, H.U., 2002. Electron spin resonance and radiocarbon dating of coral deposited by Holocene tsunami events on Curacao, Bonaire and Aruba (Netherlands Antilles). Quaternary Science Reviews, 22, 1305-1317.

Scheffers, A., 2002. Paleotsunamis in the Caribbean: Field Evidences and Datings from Aruba, Curacao and Bonaire. Essener Geographische Arbeiten, 33, 181 pp.

Scheffers, A., 2003. Boulders on the Move: Beobachtungen aus der Karibik und dem westlichen Mittelmeergebiet. Essener Geographische Arbeiten, 35, 2-10.

Scheffers, A., 2004. Boulder Deposits – Witnesses of Storm or Tsunami Events. IGC – UK Conference, Glasgow 2004, Abstract.

Whelan, F., Kelletat, D., 2003. Analysis of Tsunami Deposits at Cabo de Trafalgar, Spain, Using GIS and GPS Technology. Essener Geographische Arbeiten, 35, 11-25.

CRITICAL EVALUATIONS FOR THE STATE OF HAWAII SUBSEQUENT TO THE 26 DECEMBER 2004 ASIAN TSUNAMI

Daniel A. Walker
Tsunami Memorial Institute
59-530 Pupukea Rd.
Haleiwa, Hawaii U.S.A.

SUMMARY

A reexamination of historic data for Pacific-wide tsunamis suggests the need for modeling the effects of potential "100-year 9.0 magnitude earthquakes" from the Western and Southwestern Pacific, and possibly from Japan. Such modeling would either confirm the reliability of existing evacuation maps for the Hawaiian Islands or indicate necessary modifications. Long term observations of human responses to tsunamis in Hawaii, and more recently in Asia, suggest that tsunami education should be required in public and private schools. Destructive local tsunamis generated by small, unfelt earthquakes have struck, and will strike, portions of the Big Island without warning unless detectors similar to those protecting the Kona Coast are installed. Government and business leaders need to continually be reminded of the destructive potential of tsunamis, as well as the limitations and requirements of the warning system. Finally, critical infrastructure should be hardened to prevent damage from salt water flooding so as to facilitate a more rapid recovery from inevitable future tsunamis.

INTRODUCTION

Several key elements are now generally recognized as contributing factors in the tragedies of the Asian tsunami. Among these are the absence of a warning system for the Indian Ocean, failure to accurately assess the risks associated with tsunamis in the Indian Ocean, the absence of a general understanding of the characteristics and destructive potential of tsunamis, little or no timely intergovernmental communications, no existing evacuation plans, and possibly little or no zoning or engineering requirements to protect structures and critical lifeline facilities. Steps are now being taken by Asian countries and the international community to address some, if not all, of these issues. Perhaps the single greatest lesson to be learned from this tragedy is, once again, the failure of scientists and government agencies to analyze situations critically and objectively so as to eliminate any biases favoring desirable conclusions. As an example, thinking prior to 26 December 2004 might have been that recorded history provided no evidence of an ocean-wide tsunami in the Indian Ocean, so such a phenomenon seemed unlikely to happen. Furthermore, even if such an event were to occur, it would more than likely be a small tsunami. Therefore, concerning the local population and visitors with such an unreasonable possibility would be unnecessary and unwise. Thus, one would arrive at an acceptable, desirable, but horribly wrong conclusion. In an effort to avoid somewhat similar mistakes, the assessments that follow are offered as critical and objective evaluations of the current status of Hawaii's tsunami preparedness.

EVALUATIONS

An Asian Type Tsunami in Hawaii

In the 20th century, the Hawaiian Islands have been struck by several large Pacific-wide tsunamis. Moment magnitudes (Mw) and runups for these events are given in Walker (2000). The largest magnitudes are 9.6 (Chile '60), 9.2 (Alaska '64), 9.0 (Kamchatka '52), 8.7 (Aleutians '65), and 8.6 (Aleutians '57). [The Mw of the Indonesian earthquake west of Sumatra that produced the Asian tsunami is reported to be 9.0. Hereafter, all magnitudes cited in this report, unless otherwise indicated, will be moment magnitudes.] With some of the largest earthquakes in recorded history among those above, along with other destructive tsunamis including the powerful and anomalous 1946 event (Mw = 8.0), "worst case" scenarios may have already been experienced in the Hawaiian Islands. Also, with an existing warning system in the Pacific, it would seem improbable that Hawaii could be "surprised" by a tsunami from a 9.0 earthquake. However, a more careful examination of the data reveals that Hawaii's experience with large ocean-wide tsunamis is limited to source areas from the circum-Pacific arc extending from Japan through Alaska and from the west coast of South America. Since other portions of the circum-Pacific arc have not generated significant tsunamis in Hawaii (i.e., greater than or equal to 1 meter), does that mean that none will be generated? Isn't this the same type of "logic" that contributed to the Asian tragedy? Perhaps. It may be reasonable to dismiss large portions of the circum-Pacific arc because of the nature of faulting (e.g., the prevalent horizontal strike-slip motions along the west coast of North

America) or the orientation of subduction zones relative to Hawaii (e.g., Central America and margins of the Pacific plate extending south of Tonga). Remaining portions of the circum-Pacific arc extend south from Japan to New Guinea and continue eastward to Tonga and Samoa (Figure 1). These predominately vertical subducting margins have many segments oriented towards Hawaii. Although large locally destructive tsunamis frequently occur in some of these regions, there is no record of significant Pacific-wide propagation for the regions shown other than for Japan. In view of the Asian tragedies, a more careful analysis of these seemingly benign portions of the Pacific may be appropriate.

The question to be asked is whether these regions have been benign in terms of significant Pacific-wide tsunamis because of a deficiency of large earthquakes or because of attenuation by the large number of extensive island groups (e.g., the Caroline, Marshall, Gilbert, Ellis, and Phoenix groups) to the east and north of some of these regions. In this investigation the magnitudes of large earthquakes are examined for differing regions of subducting margins to the west and southwest of Hawaii - generally extending from south of Japan to New Guinea and eastward through to Tonga and Samoa. To find the origin times of these earthquakes, searches were made of U. S. Geological Survey on-line data bases. Only earthquakes with either body wave, surface wave, or moment magnitudes of 7.0 or greater and focal depths of less than 100 km were used. Also, foreshocks and aftershocks were excluded. With the "Significant Worldwide Earthquakes (2150 B.C - 1994 A.D.)" data base, the only earthquakes found for the regions of interest occurred in the 20th century with most of the magnitudes being based only on surface waves from a variety of different sources. Substantially more magnitudes based on seismic moments were found in the "USGS/NEIC (PDE) 1973 - Present" data base. However, to give meaning to this study, uniformly computed moment magnitudes are needed for as much of the time period as possible. To achieve this requirement, comprehensive reevaluations of seismic moments for historic earthquakes provided in the 1900 though 1989 catalog of Pacheco and Sykes (1992) were used. A formulation given in Hanks and Kanamori (1979) was then applied to convert seismic moments to moment magnitudes. For moment magnitudes subsequent to 1989, Harvard values, if available, were used (25 earthquakes). The remaining 6 values of the 113 shown in Table 1 are USGS moment magnitudes. [Regarding the moment magnitudes already cited in this report, the Indonesian value was from Harvard and all others were from Pacheco and Sykes (1992).]

It is well known that earthquake magnitude is merely an indicator of tsunamigenic potential rather than an essential determinant of a tsunami's destructive power. Critical factors are the displacement of the ocean floor and the transmission efficiency to potential runup sites. All of the five earthquakes along the margins of the Pacific with magnitudes of 8.6 or greater in the 20th century generated significant tsunamis in Hawaii (Fig 2; Walker, 2000). However, for magnitudes of 8.0 to 8.5, only 6 of 31 earthquakes generated significant tsunamis in Hawaii. Thus, the data in Table 1 indicates a substantial deficiency of large earthquakes capable of generating significant Pacific-wide tsunamis. The question remains as to whether attenuation by islands would block the transmission of an Asian-type 9.0 Mw tsunami from these regions into other areas of the Pacific. The low magnitudes of Table 1 might suggest that such large events are unlikely and an investigation of the extent of "9.0 Mw tsunami attenuation" is unwarranted.

However, such a position is no longer tenable after 26 December 2004. Region B in Table 1, described as "West of New Guinea", is indeed far to the west of New Guinea. In fact, this region encompasses the subducting margins under, and adjacent to, Sumatra (the search grid used was 15 N to 15 S and 90 E to 105 E). The only magnitude excluded from Table 1 for this region is the 9.0 of 26 December 2004. The fact that for a span of more than 100 years the next largest magnitudes were only two 7.9's is disturbing, to say the least!

In terms of tsunamigenic potential as evidenced only by earthquake magnitudes, Table 1 indicates the western and southwestern margins of the Pacific Ocean may be as dangerous as the eastern margin of the Indian Ocean. Thus the question of "island attenuation" transforms from a questionable academic exercise to a critical and urgently needed inquiry. Modeling of a "100 year tsunami" (i.e., one generated by a 9.0 earthquake) for differing regions of the Western and Southwestern Pacific will be needed to determine whether island chain attenuation would be substantial or whether a significant Pacific-wide tsunami would, in fact, be generated. If attenuation is not substantial, inundations in some areas, especially along the southern and western shores of Hawaii, could exceed historical values from tsunamis in the North Pacific and South America. It should be noted that there are no island chains between Hawaii and the subducting margins south of Japan to Guam. Also, the largest magnitude for tsunamis recorded in Hawaii from Japan is only an 8.4 (in 1933) suggesting that the effects on Hawaii of a tsunami generated by a 9.0 earthquake in Japan should also be modeled.

Education

In addition to avoiding biases favoring acceptable, desirable, but potentially horribly wrong conclusions, an essential component of any successful warning system is education. As has occurred with teachers and students at Laupahoehoe in 1946, residents of Hilo in 1960, and hundreds of surfers on Oahu's north shore in 1994, curiosity, short-term memories, and a failure to understand the nature and destructive power of tsunamis can undermine the effectiveness of any warning system. To best overcome the realities of human nature, tsunami education should be institutionalized in public and private schools to ensure that children know the characteristics and destructive power of tsunamis, and to ensure that they and their teachers know what to do regardless of whether they are at school or elsewhere. A small amount of time dedicated to this topic on siren test days could be an effective method for achieving this objective.

Communications

Most aspects of communications are continually tested and upgraded by State and County Civil Defense agencies, as well as the Pacific Tsunami Warning Center. However, one perceived glaring deficiency in communications is likely unless corrective actions are taken. Because of an absence of instrumentation along parts of the Puna and Kona coastline from Punaluu to Kapoho, a small unfelt earthquake could generate a highly localized but destructive tsunami along shorelines popular with residents and tourists (i.e., Punaluu, Pohoiki, and Ahalanui), and in coastal campground areas of the

Hawaii Volcanoes National Park. No warnings would be possible in those areas for such a tsunami although some other shorelines at risk on the Big Island are instrumented with devices (i.e., along the Kona Coast from Honokohau to Milolii) that would detect such tsunamis and provide Civil Defense personnel with an opportunity to sound warning sirens. History confirms that such a tsunami will occur (Walker and Cessaro, 2002). Instruments will have to be installed sooner or later. Will this be done before or after such a tsunami? If "after", the public will ask why a technologically possible warning was not given to them - thus a major communications and credibility problem for State and County leaders, Civil Defense agencies, and the Pacific Tsunami Warning Center.

Warnings

Potential problems with warnings are related to instrumentation, education, and communication issues. Until data from the National Oceanic and Atmospheric Administration's tsunami buoys, or from some other as yet undiscovered methodology, has a substantial history of success, warnings perceived as "false" by the public are always a possibility. People of Hawaii need to understand the limitations of our warning system. They need to know that once the reliability of data used in the warning system is established, false warnings will be reduced or eliminated. Also, for some warnings only limited evacuations may be required (Walker, 2004) resulting in a substantial reduction in business losses to our economy. Not only does Hawaii have a warning system for Pacific-wide tsunamis but, as has already been mentioned, a warning system for locally generated tsunamis for part of the Big Island. This system also provides an early warning for the rest of the State should a large tsunami occur on the Kona Coast. Historical data and the successful operation of the tsunami sensors on the Kona Coast suggest that local warning criteria should be reviewed to eliminate overcautious, and obviously false, local warnings. Also, some criteria might be eliminated so that warnings can be called more quickly. Necessary upgrades and expansions of the local warning system should be made. The people of Hawaii need to understand the differences and characteristics of both Pacific-wide and local warnings.

Infrastructure

There may be no justification for the destruction of critical facilities by salt water flooding. In some areas most of the potential flooding damage will be the result of a gradual increase in water level rather than powerful horizontal surges. Earthen berms, sandbags, or waterproof doors could prevent much of this damage. In other areas more drastic protection may be required. Government agencies should be sure that such critical lifelines (i.e., electrical, water, sewage, fuel, communications, fire, police, and transportation) are "hardened" not only for tsunamis but also for hurricanes. These suggestions have previously been made for Hawaii, and generally ignored, in a U. S. Army Corps of Engineers Report (1999).

CONCLUSIONS

The following recommendations should be urgently adopted as "action items" with strategies and timelines. (1) Proactive government agencies should implement modeling to determine the effect on Hawaii of a "100-year 9.0 magnitude earthquake" from regions in the Western and Southwestern Pacific, including Japan. (2) The local warning system should be expanded and upgraded. (3) The State Department of Education and other educational institutions should be encouraged to implement standardized tsunami education in their schools. (4) Warning criteria for local earthquakes should be reviewed. (5) If necessary, critical facilities managers should be made aware of tsunami hazards and be required to harden their facilities against salt water flooding. (6) Finally, our government leaders need to understand the potential impact of tsunamis on our people and economy so as to minimize losses and speed recovery in the next large tsunami. Anything less than these actions and we will have learned little from the tragedies of 26 December 2004.

ACKNOWLEDGMENTS

I thank my colleagues at Civil Defense, the Pacific Tsunami Warning Center, the International Tsunami Information Center, the University of Hawaii, the Pacific Tsunami Museum, and other tsunami researchers, past and present, for their dedication to the improvement of tsunami warnings in Hawaii.

REFERENCES

Hanks, T. C., and H. Kanamori (1979). A moment magnitude scale, J. Geophys. Res., 84, 2348-2350.

Pacheco, J. F., and L. R. Sykes (1992). Seismic moment catalog of large, shallow earthquakes, 1900 - 1989, Bull. Seism. Soc. Am., 82, 1306-1349.

U. S. Army Corps of Engineers - Honolulu Engineer District (1999). Coastal Hazard Mitigation Study for Energy and Lifeline Facilities, prepared for the State of Hawaii - Department of Business, Economic Development and Tourism, 22 pgs. with appendices.

Walker, D. A. (2000). Twentieth century Ms and Mw values as tsunamigenic indicators for Hawaii, Sci. of Tsunami Hazards, 18-2, 69-76.

Walker, D. A. (2004). Shoreline modeling segments in the Hawaiian Islands critical for regional tsunami evacuation determinations, Sci. of Tsunami Hazards, 22-2, 69-73.

Walker, D. A., and R. K. Cessaro (2002). Locally generated tsunamis in Hawaii: a low cost, real-time warning system with world wide applications, Sci. of Tsunami Hazards, 20-4, 177-186.

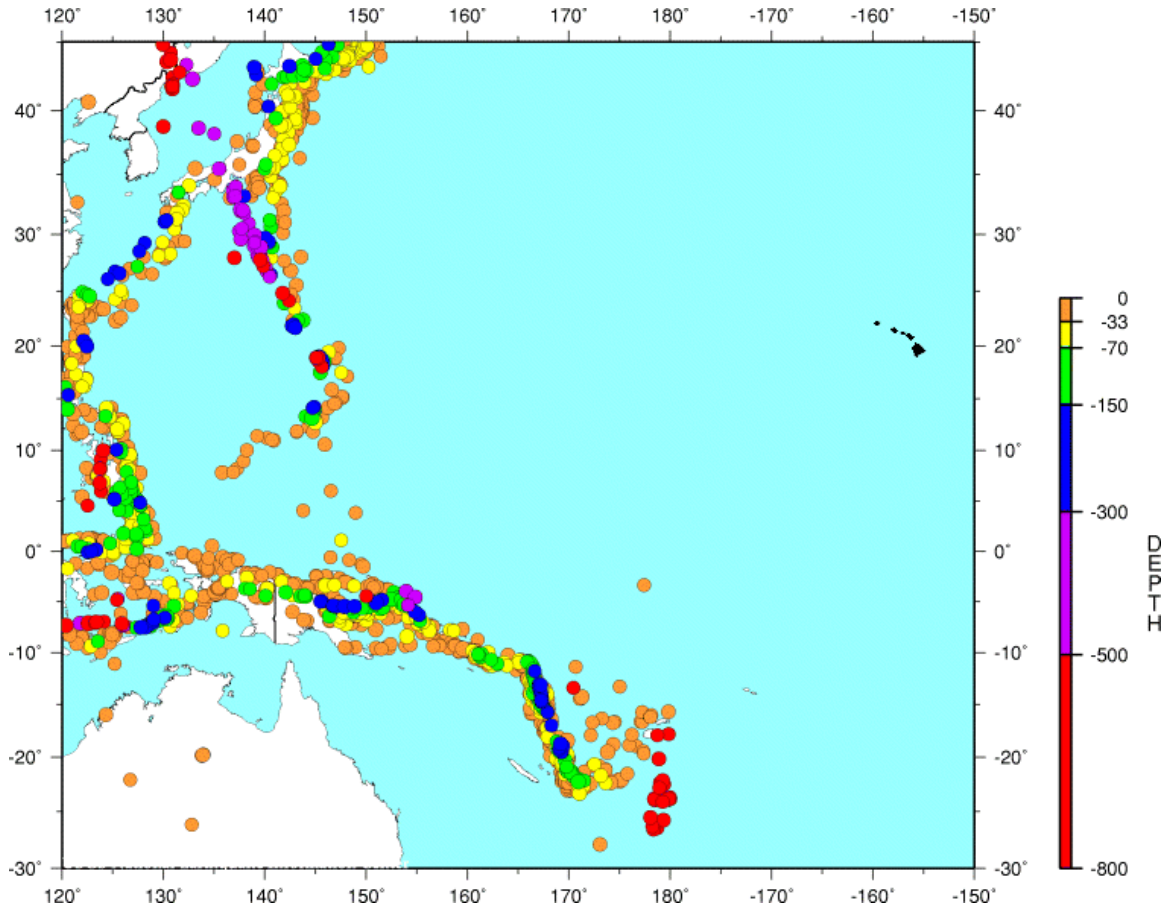

Figure 1. Subducting margins of the Western and Southwestern Pacific. Plot taken from the "USGS/NEIC (PDE) 1973 - Present" on-line data base for all magnitudes greater than or equal to 6.0.

TABLE 1

Moment Magnitudes for Subducting Margins to the West and Southwest of Hawaii (1900 - 2004) for Earthquakes with Focal Depths of Less than 100 Kilometers*

Moment Magnitude	Region							
	A	B	C	D	E	F	G	H
7.0	x	x	x	xxx	xxxx		xxx	x
7.1	x	x	x	xx	xx	xxx	xxx	
7.2				x	xxx	x	xxxx	x
7.3		xx	xx	xxx	x	x	xx	x
7.4	xxxx	xxx	x		x	xx		xx
7.5	xx	xx	x	x	xxxx	xxx	xx	x
7.6	x			x	xxx	xx		x
7.7		x	x		xx		xx	x
7.8	x	x				xxx	xx	
7.9	x	xx	x					
8.0			x	x	x			
8.1	xx				x			
8.2			x					
8.3								x
8.4								
8.5								x
8.6								
8.7								
8.8								
8.9								
9.0								

* Regions investigated are: (A) - Western Pacific; (B) - West of New Guinea; (C) - Western New Guinea; (D) - Eastern New Guinea; (E) - Western Solomons; (F) - Eastern Solomons; (G) - Santa Cruz; and (H) - Tonga/Samoa. Grids used to search the on-line U.S. Geological Survey/National Earthquake Information Center data bases will be provided upon request.

THE EARTHQUAKE AND TSUNAMI OF NOVEMBER 21, 2004 AT LES SAINTES, GUADELOUPE, LESSER ANTILLES

Narcisse Zahibo[1], Efim Pelinovsky[2], Emile Okal[3], Ahmet Yalçiner[4], Christian Kharif[5], Tatiana Talipova[2], and Andrey Kozelkov[6]

[1] Laboratoire de Physique Atmosphérique et Tropicale, Département de Physique, Université Antilles Guyane, Pointe-a-Pitre, France (E-mail: narcisse.zahibo@univ-ag.fr)
[2] Laboratory of Hydrophysics and Nonlinear Acoustics, Institute of Applied Physics, Nizhny Novgorod, Russia (E-mail: pelinovsky@hydro.appl.sci-nnov.ru)
[3] Department of Geological Sciences, Northwestern University, Evanston, USA (Email: emile@earth.northwestern.edu)
[4] Civil Engineering Department, Ocean Engineering Research Center, Middle East Technical University, Ankara, Turkey (E-mail: yalciner@metu.edu.tr)
[5] Institut de Recherche sur les Phénomènes Hors Equilibre (IRPHE), Technopôle de Château-Gombert, Marseille, France (E-mail: kharif@irphe.univ-mrs.fr)
[6] Applied Mathematics Department, State Technical University, Nizhny Novgorod, Russia (E-mail: ask_nnov@mail.ru)

ABSTRACT

A strong earthquake (m_b = 6.3; M_s = 6.1; M_w = 6.3) occurred on 21 November 2004 in the Dominica Passage separating Guadeloupe and Dominica, in the Lesser Antilles, and generated a weak tsunami with maximum amplitudes of +70 and -80 cm on neighbouring islands. We conducted field surveys on the islands of "Les Saintes", in the immediate vicinity of the epicenter on November 27, 2004 and February 12, 2005, and report here on the resulting dataset.

1. Introduction

The earthquake which occurred on November 21, 2004 at 11:41:07 UTC (07:41 local time) in the Dominica Passage, Lesser Antilles (Figure 1) was the strongest in this area since 1969. Preliminary epicentral coordinates given by the National Earthquake Information Center of the U.S. Geological Survey are 15.677°N, 61.650°W, with a focal depth of 14 km, and conventional magnitudes m_b = 6.3, M_s = 6.1. The USGS Moment Tensor Solution has a moment of 3.2×10^{18} Nm (M_w = 6.3), and a centroid location at 15.681°N, 61.693°W, 6 km depth; its focal geometry is: strike ϕ = 327°, dip δ = 35°, slip λ = -92°. The Harvard CMT inversion yields a comparable geometry (ϕ = 317°; δ = 44° deg. λ = -88°) with a moment of 3.35×10^{18} Nm and a centroid at 15.81°N, 61.63°W with a depth of 12 km. Thus the earthquake is readily interpreted as a shallow normal faulting event taking place in the back-arc; the slight deficiency of M_s relative to m_b could be indicative of a somewhat fast strain release, suggestive of a higher-than-normal stress drop. This is further supported by the analysis of estimated energy (Newman and Okal, 1998), which yields a slowness parameter Θ = -4.59, slightly greater than predicted by scaling laws (-4.90). As of the time of writing, the earthquake had 8 aftershocks with $m_b \geq 5$, the latest and largest aftershock to date (m_b = 5.7 on February 14, 2005) having inflicted additional damage in the epicentral area.

Figure 1. Map of the Caribbean basin showing the location of the earthquake of November 21, 2004.

A five-year old girl was killed and two other persons injured in Trois-Rivières (Guadeloupe, approximately 35 km from the epicenter; see Figure 1 for locations). One person was injured in Capesterre (Guadeloupe) and ten people suffered minor injuries in Petites-Anses (Island of Terre–de-Bas, Les Saintes, 20 km from the epicenter). Many buildings were destroyed or damaged in locations as far away as Pointe-à-Pitre, 65 km away from the epicenter, as well as in Portsmouth, Dominica (25 km from the epicenter; see Figures 2-4). To the North, the earthquake was felt in Antigua and Barbuda (150 km) and St Kitts and Nevis (190 km) and to the South as far away as Saint Lucia (220 km). This event was widely discussed and commented in the local newspaper "France-Antilles" (Guadeloupe) and on local television. However, any information about the possible generation of a tsunami by the earthquake was notably absent from media reports, which motivated the field surveys carried out in the aftermath of the event. We give below a sample of photographs and witness reports.

Figure 2. Houses at Trois-Rivières, Guadeloupe damaged during the earthquake (Photographs by N. Zahibo and A. Yalçıner). In the last photograph, the islands of Les Saintes, where the earthquake was destructive, can be seen in the background.

Figure 3. Houses damaged by the earthquake at Petites-Anses, Terre-de-Bas Island (Les Saintes, Guadeloupe; Photographs by N. Zahibo and A. Yalçıner).

Figure 4. Roman Catholic and Methodist Churches at Portsmouth, Dominica damaged during the earthquake (Wayne Abraham, http://dominicapsn.freeyellow.com/gallery.html).

2. Background: historical tsunamis in Guadeloupe and Dominica

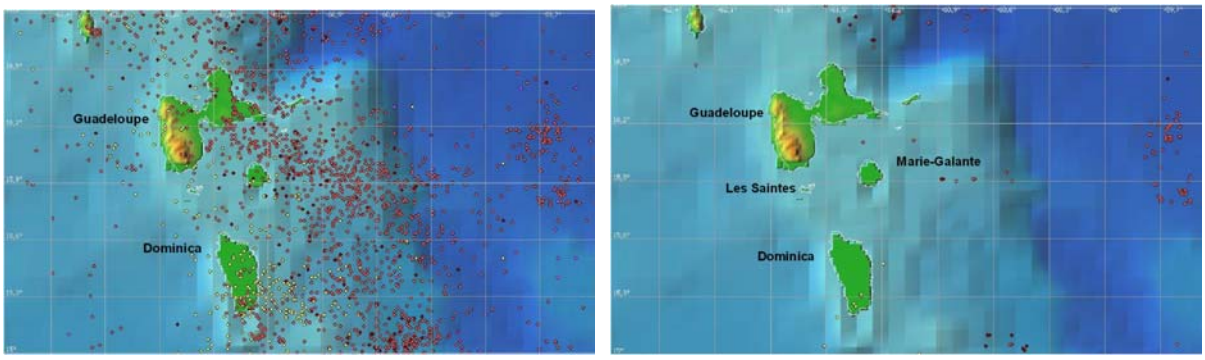

Figure 5. Seismicity of Guadeloupe and Dominica (left), and distribution of earthquakes with magnitudes greater than 5.0 (HTDB/ATL, 2002). Note that, before the November 2004 earthquake, the latter were concentrated at the trench.

As documented on Figure 5 (HTDB/ATL, 2002), the seismicity of the area is generally high, but most earthquakes remain weak, with only eight events (listed in Table 1) exceeding a magnitude of 6.

Of those, the pre-instrumental event of 08 February 1843, estimated at M = 8.3 by Shepherd and Lynch (1992), occurred to the Northwest of Guadeloupe. It was disastrous in the economic capital of Pointe-à-Pitre, where 1500 people were reported killed, amounting to one-third of the population at the time, and was felt strongly (at MMI IX to X) in St Kitts, Montserrat, Martinique, St. Lucia and other islands, and was also felt as far away as Surinam, Bermuda and South Carolina. This earthquake was accompanied by a tsunami at Antigua where the sea rose 1.2 m (Lander *et al.,* 2002). However, the motion of the sea on the coast near Pointe-à-Pitre was, in fact, rather weak, the water barely inundating a few low-lying steps along the city's quays, with similar effects in Basse-Terre and Les Saintes (Guadeloupe), and in Dominica (Sainte-Claire Deville, 1867).

Table 1. List of local earthquakes with magnitude exceeding 6.0

Year	Month	Day	Lat (N)	Lon (W)	Depth	M
1843	2	8	16.5	62.2	33	8.3
1897	4	29	16.1	61.3	33	7.5
1906	12	3	15	61	100	7.9
1969	12	25	16.08	59.77	8	6.5
1969	12	25	15.79	59.7	7	7.5
1982	1	30	16.74	61.43	63	6.0
1995	3	8	16.56	59.56	8	6.3
1996	9	24	15.19	61.44	146	6.0

The earthquake of December 25, 1969 (m_b = 6.4; M_s = 7.5; $M_0 = 7.8 \times 10^{19}$ Nm; Stein *et al.,* 1982) was felt on Guadeloupe, Dominica, Martinique, St. Vincent, Antigua and Barbados. It was accompanied by a weak tsunami recorded at Barbados, Antigua and Dominica, with a maximum amplitude of 46 cm at Barbados. The single tide-gauge record of this event at Dominica (maximum amplitude 12 cm) is presented in Figure 6.

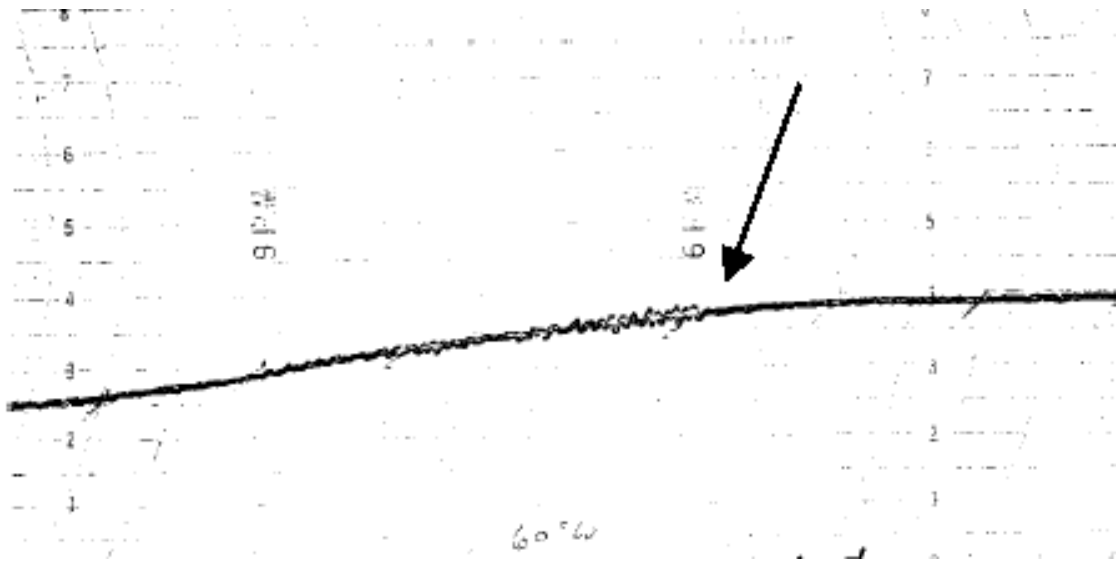

Figure 6. Tsunami of December 25, 1969 recorded at Dominica (Shepherd, 2001).

In addition, a tsunami was generated on February 17, 1843 by a submarine eruption "half-way between Guadeloupe and Marie-Galante", when a water column of 30 m was ejected from fissures in the ground (Lander *et al.,* 2003).

All other tsunamis reported to have reached Guadeloupe and Dominica originated from distant earthquakes. The first such event is the strong earthquake at Lisbon, Portugal on November 1, 1755, whose tsunami was recorded throughout the Caribbean, from Barbados to Cuba, with run-up reported to have reached 3.6 m at Samana Bay, Dominica (Lander *et al.,* 2002).

The tsunami from the strong earthquake of November 18, 1867 in the Virgin Islands (with an estimated magnitude of 7.5) was recorded in Guadeloupe with an amplitude of about 10 m at Deshaies and only 1 m at Basse-Terre and Fond Curé (Terre-de-Haut, Les Saintes; Zahibo and Pelinovsky, 2001); this event was modelled by Zahibo *et al.* (2003).

A moderate earthquake (m_b = 6.3; M_w = 6.3) occurred on March 16, 1985, causing damage and injuries to six people in Guadeloupe; a tsunami reaching several centimeters was recorded at Basse-Terre, Guadeloupe (Lander *et al.,* 2002).

The last tsunami recorded in Guadeloupe before 2004 took place on 13 July 2003, when a wave with an amplitude of about 1 m reached Deshaies (Northern Guadeloupe), following the penetration of the sea by a large pyroclastic flow during the volcanic eruption at Montserrat, 65 km away (Pelinovsky *et al.,* 2004).

In conclusion, at least seven verified occurrences of tsunamis took place in Guadeloupe and Dominica between 1843 and 2003, most of them originating from submarine earthquakes. Taking into account that strong earthquakes with magnitude greater than 7.0 occurred in this area in the past 200 years, and also the documented hazard from distant tsunamis, we may conclude that the probability of a large tsunami at Guadeloupe in the future is high.

3. Field surveys of the 2004 Les Saintes tsunami

Unfortunately, no instrumental records of the 2004 tsunami are available, since no tide gauges are presently operational in Guadeloupe. (One such instrument did operate in the past at Basse-Terre, and provided a record of the 1985 tsunami.) In addition, a heavy storm took place on the day of the earthquake (November 21, 2004), and prevented the observation of weak oscillations of the sea level, as witnesses reported what turned out to be mostly storm surges, especially on the coast of the island of Marie Galante.

We conducted our field inspection at Trois-Rivières (Southern Guadeloupe) on November 23, 2004, two days after the earthquake and found the first witness of the tsunami in this coastal location. Detailed surveys took place on November 27, 2004, and on February 12, 2005.

Basse-Terre (part of the main Island of Guadeloupe) (see Figure 7 for location of all points, and tsunami heights in cm).

Figure 7. Map of the main island of Guadeloupe.

Village of Trois-Rivières. One person (a 5-year old girl) was killed, at least two other injured, and several houses destroyed or damaged in this village (Figure 3). In the port (15°58'084N, 61°38'695W), one fisherman reported that his boat dropped down about 50 cm during the earthquake and then rose back; he was afraid his boat could hit the sea bottom and tip over. A panorama of this port is shown in Figure 8.

Figure 8. Panorama of the port of Trois-Rivières, where the reported tsunami depression was about 50 cm

Marina de Rivière Sens (city of Basse-Terre). One witness informed us that the water dropped down a few cm and then rose back during the earthquake. A panorama of the beach where the tsunami was recorded is shown in Figure 9.

Figure 9. Panorama of the Marina de Rivière Sens, where the tsunami was reported as a weak depression.

Island of Terre-de-Bas, Les Saintes (see Figure 10 for location of points and wave amplitudes).

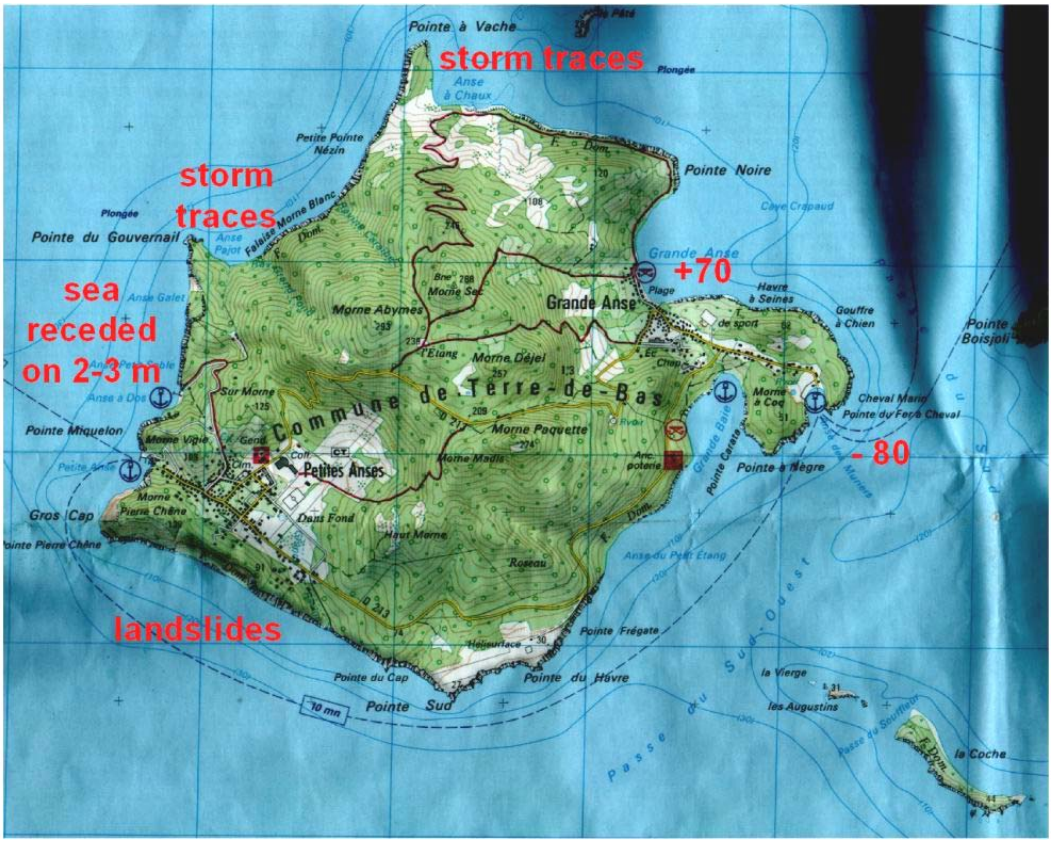

Figure 10. Map of Terre-de-Bas Island.

Village of Grande Anse, Bay "Anse des Muriers" (15°51'260N, 61°36'968W). A ship captain reported that 3 minutes after the earthquake, the sea receded 5 m (and dropped 80 cm) and rose back to its still level, over perhaps 1 minute. Photographs of this bay are given in Figure 11.

Figure 11. Panorama of the bay and interview of the tsunami witness in Bay "Anse des Muriers".

Figure 12. Panorama of the bay "Grande Anse", and interview with restaurant owner (left); the tsunami reached the house on the beach (right).

Beach of Grande Anse (15°51'547N, 61°37'476W). A restaurant owner informed us that the tsunami began as an ebbing phase, and then a positive wave reached a house on the beach; we surveyed this run-up as 70 cm (see Figure 12). According to this witness, the wave shape was

like an undular bore, which could have resulted from significant wave dispersion on this locally very gently sloping beach.

Village of Petites Anses. At least eight houses were destroyed and twenty-five damaged in this village (Figure 3). At the small bay "Anse à Dos" (see Figure 10 for location), a fisherman said that water receded a distance of 2 to 3 m just after the earthquake, and then rose back to normal level.

Bay "Anse Pajot" (see Figure 10 for location). A watermark at a height of about 50 cm was found on February 12, 2005 during the second survey around Terre-de-Bas (Figure 13). Early observation of these traces by local inhabitants suggests their deposition by storm surges, even though no major precipitation occurred since the day of the tsunami.

Figure 13. Watermarks in the bay "Anse Pajot".

Bay "Anse à Chaux" (see Figure 10 for location). Large watermarks are also visible on the beach in this bay (Figure 14). Here again, storm surges are preferred as their origin. According to reports from fishermen, storm waves approach mainly from the North, and this explains why such watermarks would be found only in those two bays, favorably open to the prevailing winds.

The southwest part of the coast, between capes "**Pointe-Sud**" and "**Gros Cap**" (see Figure 10 for location), facing directly towards the earthquake epicenter, features many fresh rockslides and landslides (Figure 15), identified by local residents as triggered during the earthquake. There, the coast is locally very steep (with cliffs as high as 30 m), and the identification of potential tsunami deposits is thus very difficult. On the South-east coast, from "Grande Baie" to "Pointe Frégate", the beach is lower (Figure 16), but we could not find definitive tsunami traces.

Figure 14. Visible traces of the wave runup in the bay "Anse à Chaux".

Island of Terre-de-Haut, Les Saintes. As one witness reported, an "unusual" surge was observed in "Baie du Marigot" (see Figure 7 for location), but there were no reports of earthquake damage from that island.

As a complement to the tsunami dataset, we quote below a message from Mr. Wayne Abraham, an amateur seismologist on Dominica, founder/coordinator of the Dominica Public Seismic Network and webmaster of the website *http://dominicapsn.freeyellow.com*: "Ten to twenty minutes after the main 6.3 shock, credible witnesses including a retired high-school teacher and a younger high-school teacher reported a significant drawing back of the sea in the Portsmouth harbour leaving fish stranded. The younger of the two even entered the area where the sea drew back and started throwing fish back into the withdrawn sea before he was beckoned to get out as there may be a possible danger of tsunami. There were no photos of the withdrawn sea but a photo was taken just after it returned, before the second - so called – wave".

Figure 15. Locations of rock- and land-slides on the Southwest coast of Terre-de-Bas.

Figure 16. Beach on the west part of the bay "Grande Baie", Terre-de-Bas.

Finally, we would like to point that two of the authors (NZ and EP) felt the earthquake and observed the appearance of resonant water oscillations in swimming pools immediately after the earthquake. Both pools are located in the northeastern part of Guadeloupe (Pointe-à-Pitre and Baie-Mahault), and in the latter case, the water overtopped the basin walls due to the small size of the pool. The seiches were polarized in the direction of the main shock (essentially north-south).

4. Conclusion

We have presented the results of field surveys of the earthquake and tsunami of November 21, 2004 in Guadeloupe. As expected, this earthquake, with magnitude 6.3, generated only a weak tsunami with run-up not exceeding 70 cm and depressions of at most 80 cm. This event constitutes at least the seventh tsunami documented in the Guadeloupe-Dominica area. However, it is rather unique among recent events in its location as a shallow normal faulting event in the back-arc. The earthquake was remarkably destructive, notably in Terre-de-Bas, due to a combination of a tendency towards to a fast source, a shallow depth, and probably site amplification of ground motion in the sedimentary basin under Petites Anses. While the tsunami amplitudes remained minimal, this earthquake serves to emphasize the constant tsunami risk in the area, notably in view of the numerous landslides triggered by the seismic event.

Acknowledgements. NZ, EP, TT and AK were supported in this study by the EDIGE and INTAS grant (01-2156), and EP by an RFBR grant (05-05-64265). EO benefited from partial support from the National Science Foundation. The authors thank Mr. Frantz Guillaume for assistance with the organization of the boat survey around Les Saintes.

References

HTDB/ATL *Expert Tsunami Database for the Atlantics*. Version 3.6 of March 15, 2002. Tsunami Laboratory, Novosibirsk, Russia, 2002.

Lander, J.F., Whiteside, L.S., and Lockridge, P.A. A brief history of tsunami in the Caribbean Sea. *Science of Tsunami Hazards*, 2002, v. 20, 57-94.

Newman, A.V., and Okal, E.A. Teleseismic estimates of radiated seismic energy: The E/M_0 discriminant for tsunami earthquakes. *J. Geophys. Res.,* 1998, v. 103, 26885-26898.

Pelinovsky, E., Zahibo, N., Dunkley, P., Edmonds, M., Herd, R., Talipova, T., Kozelkov, A., and Nikolkina, I. Tsunami generated by the volcano eruption on July 12-13 2003 at Montserrat, Lesser Antilles. *Science of Tsunami Hazards*, 2004, v. 22, No. 1, 44-57.

Sainte-Claire Deville, M.Ch. Sur le tremblement de terre du 18 novembre 1867 aux Antilles. *Comptes Rendus, Acad. Sci., Paris*, 1867, v. 65, 1110-1114.

Shepherd, J.B. Tsunami hazard in the Eastern Caribbean. *Workshop on Volcanic and Seismic Hazards in the Eastern Caribbean* (May 28 – June 1, 2001), 2001.

Shepherd, J.B., and Lynch, L.L. An earthquake catalogue for the Caribbean, Part I., The pre-instrumental period, 1502-1990. *Paper presented to the Steering Committee, Latin American and Caribbean Seismic Hazard Programme*, April 1992, 60 pp.

Stein, S., Engeln, J.F., Wiens, D.A., Fujita, K., and Speed, R.C. Subduction seismicity and tectonics in the Lesser Antilles arc. *J. Geophys. Res.,* 1982, v. 87, 8642-8664.

Zahibo, N., and Pelinovsky, E. Evaluation of tsunami risk in the Lesser Antilles. *Natural Hazards and Earth System Sciences*, 2001, v. 1, No. 4, 221-231.

Zahibo, N., Pelinovsky, E., Yalçıner, A., Kurkin, A., Koselkov, A., and Zaitsev, A. The 1867 Virgin Island Tsunami: observations and modelling. *Oceanologica Acta*, 2003, v. 26, No. 5-6, 609–621.

NUMERICAL MODELING OF THE GLOBAL TSUNAMI:

Indonesian Tsunami of 26 December 2004

Zygmunt Kowalik, Institute of Marine Science, University of Alaska
William Knight, NOAA/NWS/West Coast and Alaska Tsunami Warning Center
Tom Logan, Arctic Region Supercomputing Center
Paul Whitmore, NOAA/NWS/West Coast and Alaska Tsunami Warning Center

ABSTRACT

A new model for the global tsunami computation is constructed. It includes a high order of approximation for the spatial derivatives. The boundary condition at the shore line is controlled by the total depth and can be set either to runup or to the zero normal velocity. This model, with spatial resolution of one minute, is applied to the tsunami of 26 December 2004 in the World Ocean from 80°S to 69°N. Because the computational domain includes close to 200 million grid points, a parallel version of the code was developed and run on a supercomputer. The high spatial resolution of one minute produces very small numerical dispersion even when tsunamis wave travel over large distances. Model results for the Indonesian tsunami show that the tsunami traveled to every location of the World Ocean. In the Indian Ocean the tsunami properties are related to the source function, i.e., to the magnitude of the bottom displacement and directional properties of the source. In the Southern Ocean surrounding Antarctica, in the Pacific, and especially in the Atlantic, tsunami waves propagate over large distances by energy ducting over oceanic ridges. Tsunami energy is concentrated by long wave trapping over the oceanic ridges. Our computations show the Coriolis force plays a noticeable but secondary role in the trapping. Travel times obtained from computations as arrival of the first significant wave show a clear and consistent pattern only in the region of the high amplitude and in the simply connected domains. The tsunami traveled from Indonesia, around New Zealand, and into the Pacific Ocean. The path through the deep ocean to North America carried miniscule energy, while the stronger signal traveled a much longer distance via South Pacific ridges. The time difference between first signal and later signals strong enough to be recorded at North Pacific locations was several hours.

Science of Tsunami Hazards, Vol. 23, No. 1, page 40(2005)

1. Basic equations and tools

To study tsunami the equations of motion and continuity are formulated in the spherical polar coordinates. λ, ϕ and R, are defined as longitude, latitude and distance from the Earth's center. If the origin of the system is located on the ocean surface, it is more suitable to introduce a vertical coordinate $z = R - R_0$. Here R_0 is the radius of Earth and is equal 6370km.

Because Earth is not exactly spherical, the equations given below will better describe the large scale motion relative to the geopotential and not to the spherical surfaces. For further discussion of this problem see Gill (1982).

The vertically averaged equations of motion and continuity in the spherical system are

$$\frac{\partial u}{\partial t} + \frac{u}{R_\circ \cos\phi}\frac{\partial u}{\partial \lambda} + \frac{v}{R_\circ}\frac{\partial u}{\partial \phi} - (2\Omega + \frac{u}{R_\circ \cos\phi})v \sin\phi = -\frac{g}{R_\circ \cos\phi}\frac{\partial \zeta}{\partial \lambda} - \frac{\tau_\lambda^b}{\rho_o D} \tag{1}$$

$$\frac{\partial v}{\partial t} + \frac{u}{R_\circ \cos\phi}\frac{\partial v}{\partial \lambda} + \frac{v}{R_\circ}\frac{\partial v}{\partial \phi} + (2\Omega + \frac{u}{R_\circ \cos\phi})u \sin\phi = -\frac{g}{R_\circ}\frac{\partial \zeta}{\partial \phi} - \frac{\tau_\phi^b}{\rho_o D} \tag{2}$$

$$\frac{\partial \zeta}{\partial t} - \frac{\partial \eta}{\partial t} + \frac{1}{R_\circ \cos\phi}\frac{\partial uD}{\partial \lambda} + \frac{1}{R_\circ \cos\phi}\frac{\partial}{\partial \phi}(Dv\cos\phi) = 0 \tag{3}$$

In the above equations, u is the velocity in the λ (E-W) direction, v denotes the velocity in the ϕ (N-S) direction, and ζ is the sea level, η is the bottom displacement, t is the time, g is Earth's gravity acceleration (g=981 cm s^{-2}), ρ is water density, and D is the total depth $D = H + \zeta - \eta$. The Coriolis parameter will be taken as $f = 2\Omega \sin\phi$. It is a function of the Earth's angular velocity $\Omega = 7.29\times10^{-5} s^{-1}$ and the latitude ϕ. The components of the bottom friction force are nonlinear functions of velocity:

$$\tau_\lambda^b = ru\sqrt{(u^2+v^2)} \qquad \text{and} \qquad \tau_\phi^b = rv\sqrt{(u^2+v^2)}$$

To simplify the bottom friction terms in eqs. (1) and (2) the following notation is introduced:

$$\frac{\tau_\lambda^b}{\rho_o D} = \frac{ru\sqrt{(u^2+v^2)}}{\rho_o D} = R_x u \tag{4a}$$

$$\frac{\tau_\phi^b}{\rho_o D} = \frac{rv\sqrt{(u^2+v^2)}}{\rho_o D} = R_y v \tag{4b}$$

The dimensionless bottom friction coefficient r is taken as 3.3×10^{-3}.

In order to identify important steps in the construction of a global numerical code we shall jot down basic numerical formulas for the spherical coordinate system. The computation will be done in a space staggered grid (C grid) given in Fig.1. The u velocity grid points denoted as horizontal bars are offset from the v velocity grid points (vertical bars). Sea level grid points are denoted by crosses. The grid size (space step) along the

E-W direction is $h_\lambda = R_\circ \cos\phi \Delta\lambda$. Index $j = 1, \ldots$ stands for the space stepping along the parallels of latitude, thus the distance along the parallels is expressed as jh_λ. As the parallels of latitudes become very small circles near the poles, this geographical region needs to be either excluded from consideration or introduced into computation through a different map projection. In this study, we exclude the poles from the computational domain. The space step along the N-S direction is $h_\phi = R_\circ \Delta\phi$. Index k stands for the space stepping along the meridians of longitude. Locations of the grid points on the sphere are given by their j and k coordinates.

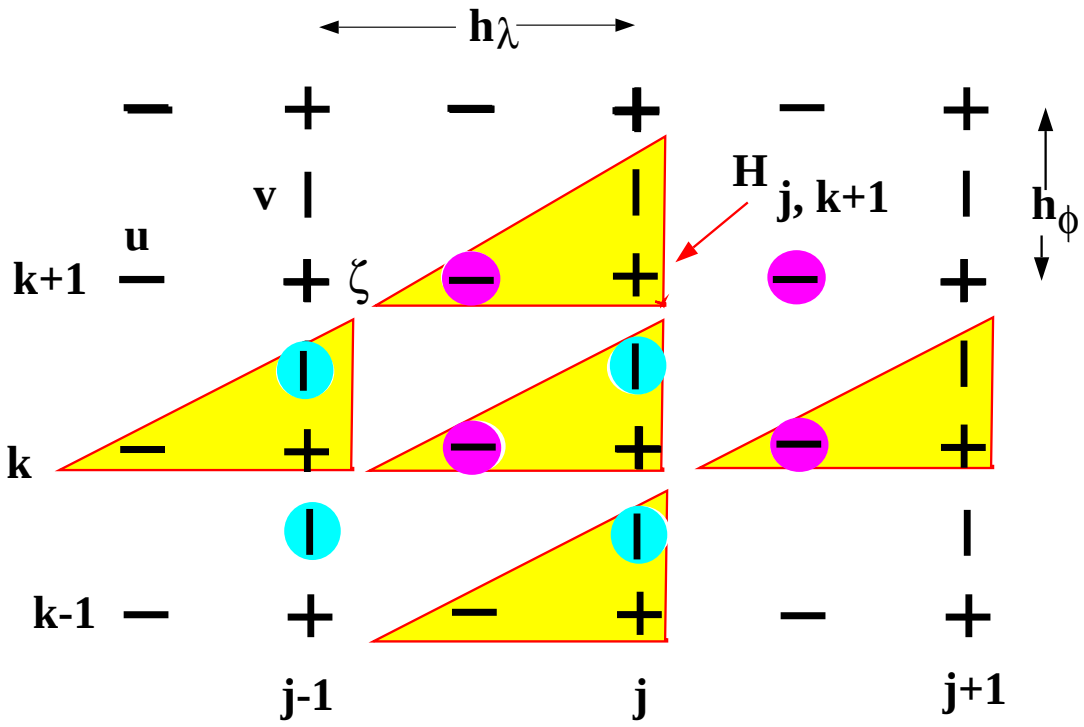

Figure 1
Spatial grid distribution in the spherical system of coordinates.

The u, v and ζ points are organized into triplets as shown by the yellow triangles in Fig.1. The depth is defined at the sea level points. To resolve some terms in the equations of motion the v velocity is needed at the u locations and vice versa. For this reason the blue and red circles are introduced to explain how the averaged values are constructed. The four values given by blue circles, when averaged will define the averaged v velocity at the u point location. This point location is given by $u_{j,k}$. The averaged v velocity at this location is $\bar{v}^u = 0.25(v_{j,k-1} + v_{j,k} + v_{j-1,k} + v_{j-1,k-1})$. In a similar way the average u velocity (four reddish circles) at the $v_{j,k}$ point is $\bar{u}^v = 0.25(u_{j+1,k}+u_{j+1,k+1}+u_{j,k+1}+u_{j,k})$.

The solution of equations(1-3) is usually advanced in time by the two-time-level numerical scheme (Kowalik and Murty, 1993; Imamura, 1996). For the spatial derivatives the second order of approximation is constructed.

$$u_{j,k}^{m+1} = u_{j,k}^{m} - \frac{gT}{h_\lambda}(\zeta_{j,k}^{m} - \zeta_{j-1,k}^{m}) + Tf\bar{v}^{u,m} + \frac{T\tan\phi_k^{\zeta}}{R_\circ}\bar{v}^{u,m}u_{j,k}^{m} - TR_{x,j,k}^{m}u_{j,k}^{m}$$
$$-\frac{u_p^m T}{h_\lambda}(u_{j,k}^{m} - u_{j-1,k}^{m}) - \frac{u_n^m T}{h_\lambda}(u_{j+1}^{m} - u_j^{m})$$
$$-\frac{T\bar{v}_p^{u,m}}{h_\phi}(u_{j,k}^{m} - u_{j,k-1}^{m}) - \frac{T\bar{v}_n^{u,m}}{h_\phi}(u_{j,k+1}^{m} - u_{j,k}^{m}) \tag{5}$$

$$v_{j,k}^{m+1} = v_{j,k}^{m} - \frac{gT}{h_\phi}(\zeta_{j,k+1}^{m} - \zeta_{j,k}^{m}) - Tf\bar{u}^{v,m+1} - \frac{T\tan\phi_k^{v}}{R_\circ}\bar{u}^{v,m}\bar{u}^{v,m+1} - TR_{y,j,k}^{m}v_{j,k}^{m}$$
$$-\frac{T\bar{u}_p^{v,m}}{h_\lambda}(v_{j,k}^{m} - v_{j-1,k}^{m}) - \frac{T\bar{u}_n^{v,m}}{h_\lambda}(v_{j+1,k}^{m} - v_{j,k}^{m})$$
$$-\frac{Tv_p^m}{h_\phi}(v_{j,k}^{m} - v_{j,k-1}^{m}) - \frac{Tv_n^m}{h_\phi}(v_{j,k+1}^{m} - v_{j,k}^{m}) \tag{6}$$

$$\zeta_{j,k}^{m+1} = \zeta_{j,k}^{m} - \frac{T}{h_\lambda}(flux_{\lambda,j+1,k} - flux_{\lambda,j,k})$$
$$-\frac{T}{cos\phi_k^{\zeta}h_\phi}(flux_{\phi,j,k} - flux_{\phi,j,k-1}) + \eta_{j,k}^{m+1} - \eta_{j,k}^{m} \tag{7}$$

In this numerical approach we aim to construct the high order of approximation in space for the continuity equation. For this purpose we expanded the upwind/downwind flux code proposed by Mader (2004). For the large scale computations the upwind/downwind is essential as it displays strong stability. We have improved the original code by an additional interpolation between the grid points and the resultant code given by eqs. 8 and 9 is close to the third order of approximation in space.

$$flux_{\lambda,j,k} = u_p^{m+1}(\zeta_{p,\lambda}^{m} - \eta_{j-1,k}^{m}) + u_n^{m+1}(\zeta_{n,\lambda}^{m} - \eta_{j,k}) + u_{j,k}^{m+1}\frac{(H_{j,k} + H_{j-1,k})}{2} \tag{8a}$$

$$\zeta_{p,\lambda}^{m} = (0.5 + u_p^{m+1}\frac{T}{h_\lambda})\zeta_{j-1,k}^{m} + (0.5 - u_p^{m+1}\frac{T}{h_\lambda})\zeta_{j,k}^{m} \tag{8b}$$

$$\zeta_{n,\lambda}^{m} = (0.5 + u_n^{m+1}\frac{T}{h_\lambda})\zeta_{j-1,k}^{m} + (0.5 - u_n^{m+1}\frac{T}{h_\lambda})\zeta_{j,k}^{m} \tag{8c}$$

$$u_p^{m+1} = 0.5 * (u_{j,k}^{m+1} + |u_{j,k}^{m+1}|) \quad \text{and} \quad u_n^{m+1} = 0.5 * (u_{j,k}^{m+1} - |u_{j,k}^{m+1}|) \tag{8d}$$

$$flux_{\phi,j,k} = \cos\phi_k^{v}\big[v_p^{m+1}(\zeta_{p,\phi}^{m} - \eta_{j,k}^{m}) + v_n^{m+1}(\zeta_{n,\phi}^{m} - \eta_{j,k+1}) + v_{j,k}^{m+1}\frac{(H_{j,k} + H_{j,k+1})}{2}\big] \tag{9a}$$

$$\zeta^m_{p,\phi} = (0.5 + v^{m+1}_p \frac{T}{h_\phi})\zeta^m_{j,k} + (0.5 - v^{m+1}_p \frac{T}{h_\phi})\zeta^m_{j,k+1} \tag{9b}$$

$$\zeta^m_{n,\phi} = (0.5 + v^{m+1}_n \frac{T}{h_\phi})\zeta^m_{j,k} + (0.5 - v^{m+1}_n \frac{T}{h_\phi})\zeta^m_{j,k+1} \tag{9c}$$

$$v^{m+1}_p = 0.5 * (v^{m+1}_{j,k} + |v^{m+1}_{j,k}|) \quad \text{and} \quad v^{m+1}_n = 0.5 * (v^{m+1}_{j,k} - |v^{m+1}_{j,k}|) \tag{9d}$$

In the above code the index m stands for the time stepping and the time step is T.

2. Domain, boundary conditions and numerical grid

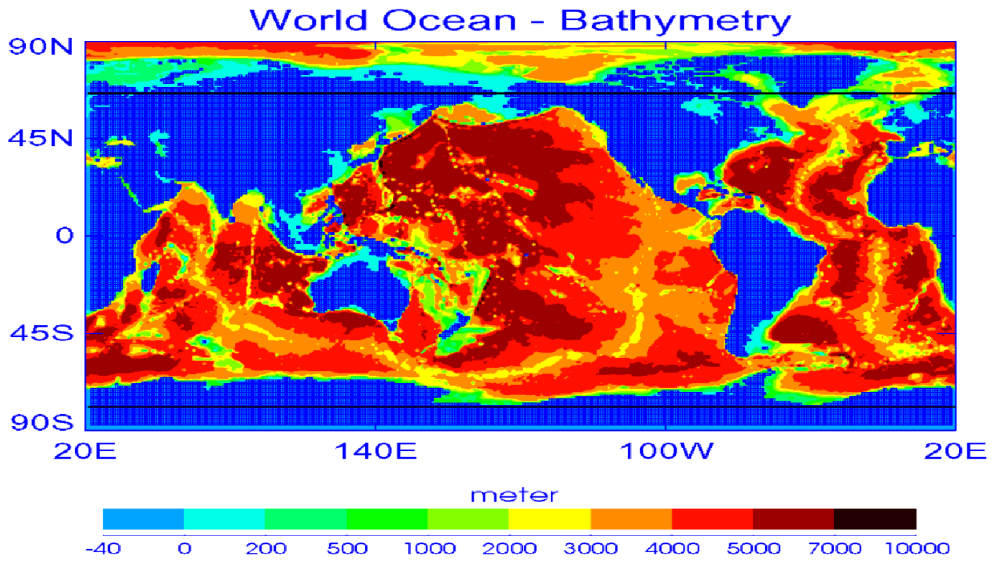

Figure 2. Ocean bathymetry. Computational domain extends from 80°S to 69°N.

The integration domain is shown in Fig.2. It extends from 80°S to 69°N. The boundaries include both wet and dry points. Along the coastal (dry points) the normal velocity is set to zero. At the wet boundary points (along 69°N) the radiation condition, established by Reid and Bodine (1968) is used. The entire globe is cut along 20°E longitude, requiring a cyclic boundary condition for sea level and the E-W velocity on this meridian. It appears at the first glance that the above boundary conditions are sufficient to derive a solution. Introductory numerical experiments show that even with the relatively large space step of 1' the new dry and wet points may be generated due to runup or run-down. A numerical scheme for the wetting and drying needs to be introduced.

The total depth $(h + \zeta - \eta)$ is usually taken as the parameter to be tested for the the presence of the wet or dry points (Flather and Heaps (1975) Immamura (1996) and

Kowalik and Murty (1993b)). The wet and dry points are identified by setting the average (undisturbed) ocean depth as positive (wet points) and elevations (dry points) as the negative values. The total depth in the dry grid points is taken as zero $D = h + \zeta = 0$. A simple runup condition is used. The following steps are taken when the dry point $(j_{wet}+1)$ is located to the right of the wet point j_{wet}.

$IF(\zeta^m(j_{wet}) > -H(j_{wet}+1))$ THEN $u^m_{j_{wet}+1} = u^m_{j_{wet}}$. If wetting is possible (as indicated by the above condition) the velocity from the wet point is extrapolated to the right (dry point), but sea level is calculated through the equation of continuity.

The spatial grid step of numerical computation is $1'$, ($R_0\Delta\phi$=1.852km) and it changes along the circle of longitude as $R_0\Delta\phi\cos\phi$. Numerical stability requires that this step be smaller than distance $T\sqrt{gH}$. The deepest point in the World Ocean (h$\simeq$11000m) is located close to 11°N therefore the time step of numerical integration is less than 7.9 s. This step was diminished to 2 s as the runup scheme requires smaller time stepping. The total number of the grid points was close to 2×10^8, therefore the simple time stepping solution, even on a supercomputer may take several weeks. The entire domain was split along the meridians into 40 subdomains to apply 40 processors. With this parallelization, 50hrs of tsunami propagation was reproduced in 9hrs of computer run time.

A small spatial step is important as the short-period waves can be obliterated during large distances of propagation when using large spatial steps. Taking the average depth of the World Ocean as 4000 m, a wave with 10 minute has a wavelength close to 120 km. Such wave length is discretized by the $1'$ grid into about 64 mesh lengths. The amplitude of a sinusoidal wave propagating over distance 10000 km will diminish only about 2%, and some shorter dispersive wave will be generated as well (Kowalik, 2003).

3. Source function

The generation mechanism for the Indian Ocean tsunami is mainly the static sea floor uplift caused by abrupt slip at the India/Burma plate interface. Permanent, vertical sea floor displacement is computed using the static dislocation formulae from Okada (1985). Inputs to these formulae are fault plane location, depth, strike, dip, slip, length, and width as well as seismic moment and rigidity. The earthquake's total rupture extent can be estimated by several approaches. Finite fault seismic data inversion is one method which yield fault lengths on the order of 350km to 650km (e.g. Ji, 2004; Yagi, 2005). Another traditional method to delineate earthquake fault zones is plotting the aftershocks which occur in the first 24 hours following the main shock. The aftershocks are expected to cluster within the slip zone. This approach leads to an estimate of 1200km for the fault length (NEIC, 2004). In this study, the fault extent is constrained by observed tsunami travel times to the northwest, east, and south of the slip zone. Figure 3 displays the tsunami arrival time constraints on the fault zone. Tsunami arrival times at Paradip-India (SOI, 2005), Ko Tarutao-Thailand (Iwasaki, 2005), and Cocos Island (Merrifield et al., 2005) tide gages are plotted in reverse. That is, the observed travel time contour is plotted with the tide gage location as the origin point. This method indicates a fault zone approximately 1000km by 200km. The epicenter location lies on the southern end of the fault zone.

To accommodate trench curvature, the fault plane is broken into two segments. Fault parameters for the two segments are listed in Table 1. Strike, dip, and slip are based on the

definitions from Aki and Richards (1980). Strike is determined by the trench orientation. Dip is taken from the Harvard CMT solution (HRV, 2005). The slip for the southern segment is based on the Harvard CMT solution while slip for the northern segment is set at 90° based on observed tsunami first motions on Indian tide gages (NIO, 2005). Depth is based on the finite fault inversion of Ji (2004). The total moment release (derived by assuming an average slip of 13m and rigidity of 4.2×10^{11}dyne cm^{-2}) in the two segments equals 1.08×10^{30} dyne cm (Mw=9.3) which is in good agreement to 1.3×10^{30} dyne cm proposed by Stein and Okal (2005) based on normal mode analysis.

Table 1. Fault parameters used to generate vertical sea floor movement.

Earthquake Parameter	Southern Fault Segment	Northern Fault Segment
Strike	335°	350°
Dip	8°	8°
Slip	110°	90°
Length	300 km	700 km
Depth (SW corner)	8 km	8 km
SW corner Latitude	3.0N	5.6N
SW corner Longitude	94.4E	93.3E
Moment	3.2×10^{29}dyne cm	7.6×10^{29}dyne cm
Rigidity	4.2×10^{11}dyne cm^{-2}	4.2×10^{11}dyne cm^{-2}

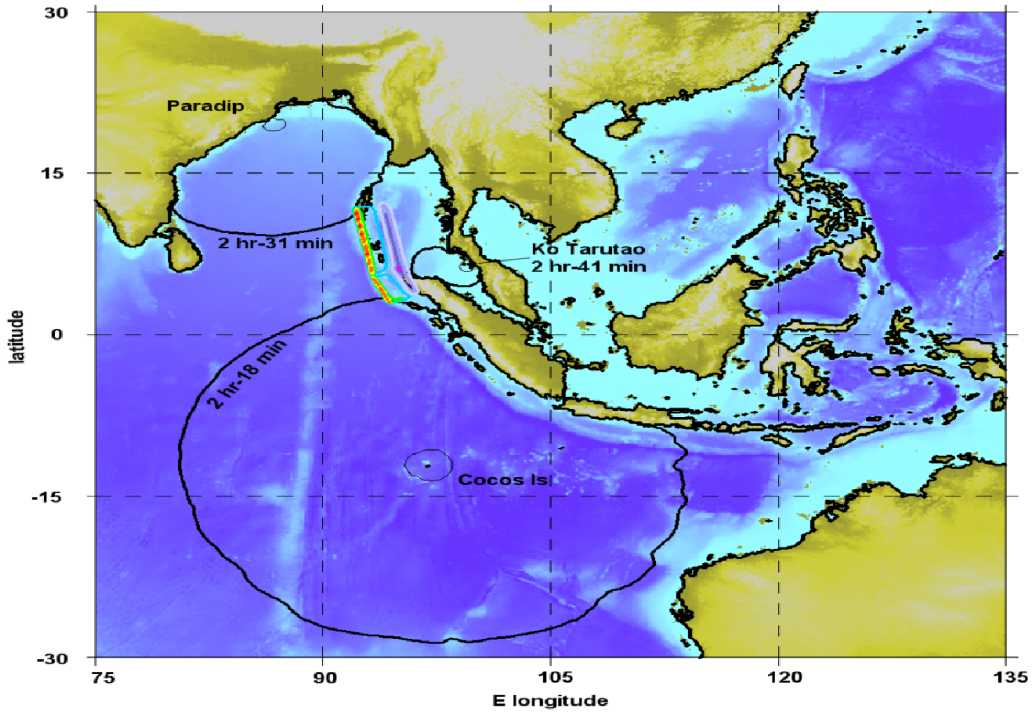

Figure 3. December 26, 2004 Sumatra earthquake uplift as constrained by tsunami travel times.

The contours of the source functions are given in Fig.4.

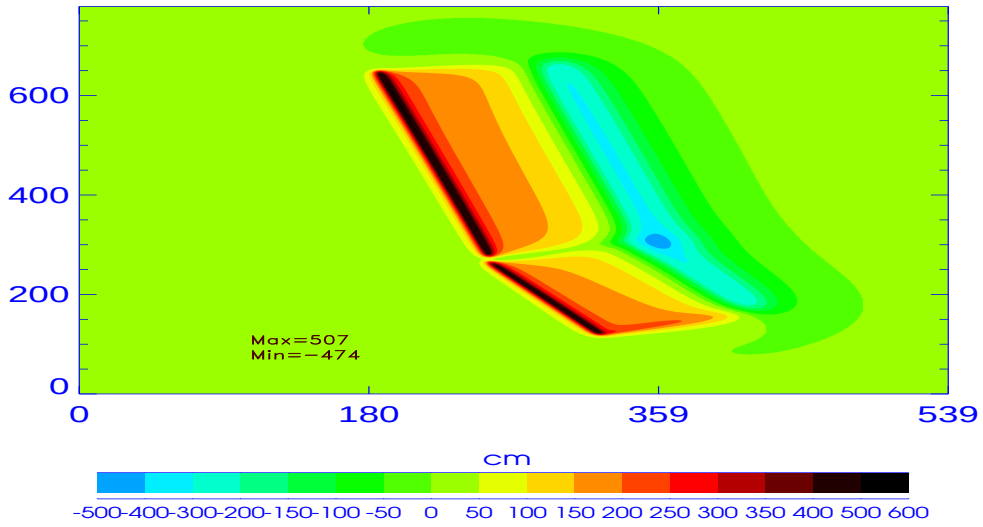

Figure 4. The source deformation contours. Maximum uplift is 507 cm and maximum subsidence approximately 474 cm. Coordinates are given in geographical minutes. Point (0,0) is located at 89°E and 1°N.

The total potential energy related to the bottom deformation given in Fig. 4 which is transferred to the sea level oscillations is calculated as

$$E_p = 0.5 \int \int \rho g \zeta^2 R_\circ^2 \delta\phi\delta\lambda$$

Calculation over the area of deformation sets the potential energy to 5.39×10^3TJ (terra joule).

4. Global distribution of maximum amplitude.

Model computations using the above source were made for the 50 hrs of propagation so that the tsunami signal could travel over the entire World Ocean. During this computation the maximum tsunami amplitude in every grid point was recorded. The plot of maximum amplitude in the proximity of the generation domain is given in Figure 5 and the corresponding plot for the World Ocean is given in Figure 6. The strongly directional signal generated by the elongated source dominates the Indian Ocean domain. The main energy lobe is directed towards Sri Lanka and the secondary lobe points towards South Africa, sending a strong signal into the Atlantic Ocean. The maximum amplitude is 15.5m in proximity to the fault, 9.3 m at the shore of Thailand, 8.1 m at Sri Lanka, and 3.3 m at the coast of East Africa.

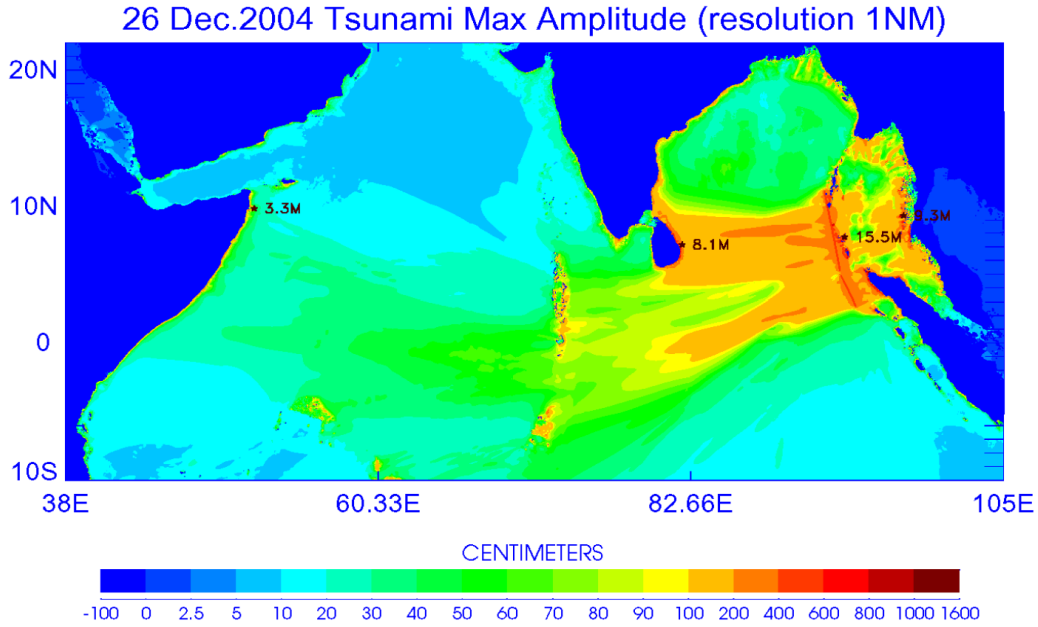

Figure 5. Maximum amplitude in the Indian Ocean.

This figure also depicts the amplitude enhancement in the shallow water and especially in proximity to peninsulas and islands due to energy concentration through the refraction process. The large domain of the Arabian Sea is located in the shadow of the main energy beam. Both computation and observation demonstrate significant increase of the tsunami amplitude up to 1.5 m at the coast of Oman at tide gauge in Salalah.

This global maximum amplitude distribution (Figure 6) shows that the Indonesian tsunami traveled all over the World Ocean. Although the source directivity pushed most of the wave energy towards South Africa, nonetheless quite a strong signal is directed towards the Antarctica. It is easy to see by checking the bathymetry that tsunamis tend to propagate towards Antarctica along the oceanic ridges and subsequently continues to transfer higher energy along the South Pacific ridge towards South and Central America. This mode of propagation brings the tsunami amplitude up to 65cm along the Pacific coast of South America. A similar mode of energy transfer is observed in the Atlantic, where the Mid-Atlantic Ridge channels the tsunami to produce 30cm wave amplitude as far north as Nova Scotia. An especially large energy flux is ducted from the South Atlantic Ridge towards Brazil and Argentina. The filaments of energy trapped along the South Pacific Ridges are most spectacular as they duct tsunami energy for many thousands of kilometers. A simple explanation of the energy trapping using the continuity equation leads us to conclusion that the amplitude should increase over the ridges due to shallower depth. At the same time the role of the bottom friction over the 2km deep ridge is negligible and therefore the tsunami can travel long distance without energy losses.

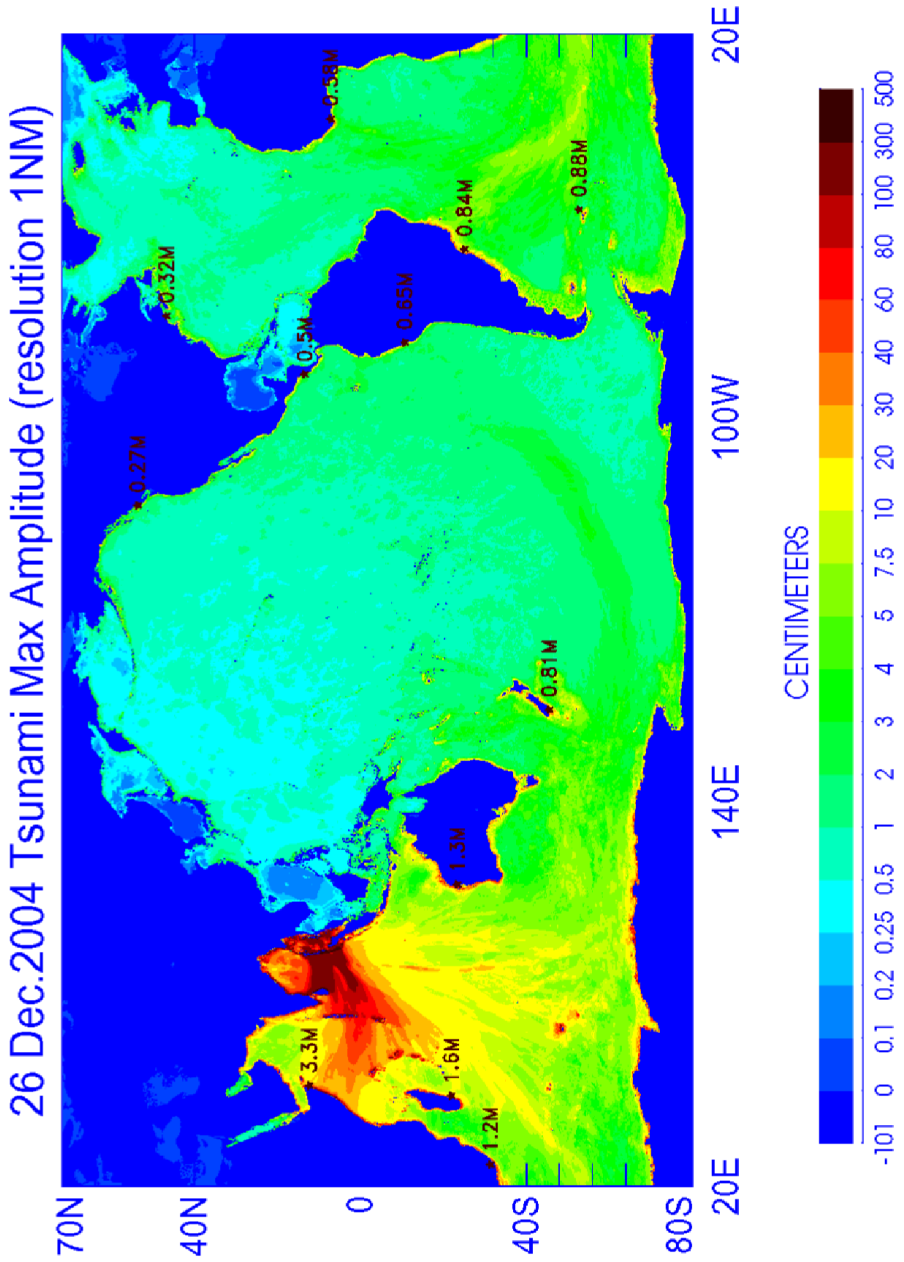

Figure 6. Maximum amplitude in World Ocean.

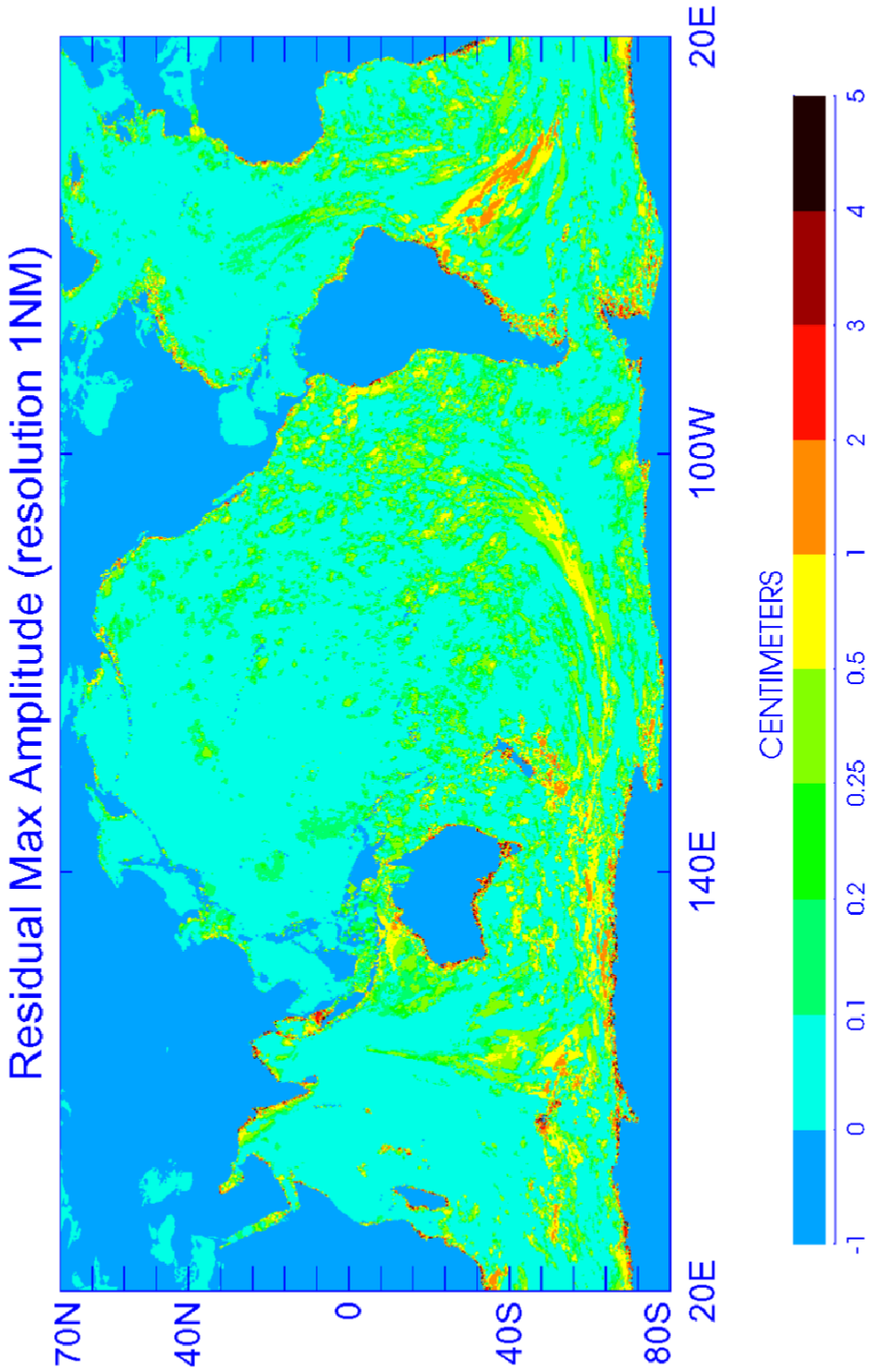

Figure 7. Residual maximum amplitude in World Ocean.

The trapping of this energy is probably related to the long waves trapped along the ridge (Mei, 1989). The cross-ridge trapping length, which is responsible for energy concentration, is approximately defined by the tsunami wavelength. As the Indonesian tsunami carried a wide spectrum of waves with periods from 20 to 50min, the wavelength for the mid-ocean travel is in the range of 100km to 600km. A simple explanatory model for the long wave trapping may be based on different speed of the tsunami wave over and off ridge. As the wave over ridge is slower and wave off ridge is faster, the joint tsunami wave front is curved in such a way that the energy is fluxed towards the ridge.

The above explanation neglects the influence of the Coriolis force on tsunami propagation. Tsunamis are typically computed without Coriolis force because their periods are much smaller than the inertial period. As propagation proceeds over long distances the compounding effect of Coriolis force may sum up and increase. In Fig. 7 the residual maximum amplitude is given as difference between two computed distribution, with and without Coriolis force. The difference given in Fig. 7 shows locations where Coriolis force dominates. The amplitudes are not very large and according to expectation the influence is increasing towards the south since the Coriolis term increase poleward from equator. Consistent change is observed along the South Pacific Oceanic Ridge. Residuals due to Coriolis force are close to 1cm and since the total amplitude along this ridge according to Fig. 6 is approximately 4cm, we may conclude that Coriolis force plays a certain role in the energy trapping along the oceanic ridges (see also trapping in the South Atlantic). A simple model for energy trapping due to the Coriolis force is a Kelvin wave propagating along the depth discontinuity (Longuet-Higgins, 1969). The across-discontinuity trapping distance is defined by the Rossby radius of deformation (Gill, 1982). This distance is a function of depth and latitude and for the depth from 1km to 4km and for latitude of 40° to 60° the Rossby radius ranges from 1000km to 2000km. As this length is much larger than the tsunami wavelength we can conclude that Coriolis force is less effective in the concentrating tsunami energy along the oceanic ridges.

5. Travel time.

Tsunami travel time from the source region to the given location is important parameter in the tsunami prediction and warning. The Indonesian tsunami arrival times have been determined for many locations (Merrifield et al,2005; Rabinovich, 2005; http://www-sci.pac.dfo-mpo.gc.ca/osap/projects/tsunami/tsunamiasiax_e.htm; http://ilikai.soest.hawaii.edu/uhslc/iotd/; http://www.nio.org/jsp/tsunami.jsp). This set of data presents a possibility for the ocean-wide comparison of the data and the model. The first numerical experiment delineates the tsunami arrival time at every grid points for a signal of 0.1cm amplitude. The computed tsunami travel time chart is depicted in Fig. 8. The chart shows that even at such small limiting amplitudes the tsunami signal arriving at Alaska and North America did not pass through the Indonesian Straits but rather around the Australia and New Zealand.

The next numerical experiment computes isolines of arrival time for the tsunami signal of 0.5cm amplitude (Figure 9). In the vast regions of Northern and Central Pacific this figure does not show a consistent arrival time. We may conclude that the main premise used to construct these figures, namely that the first train of tsunami waves is associated

with the largest wave, does not hold true.

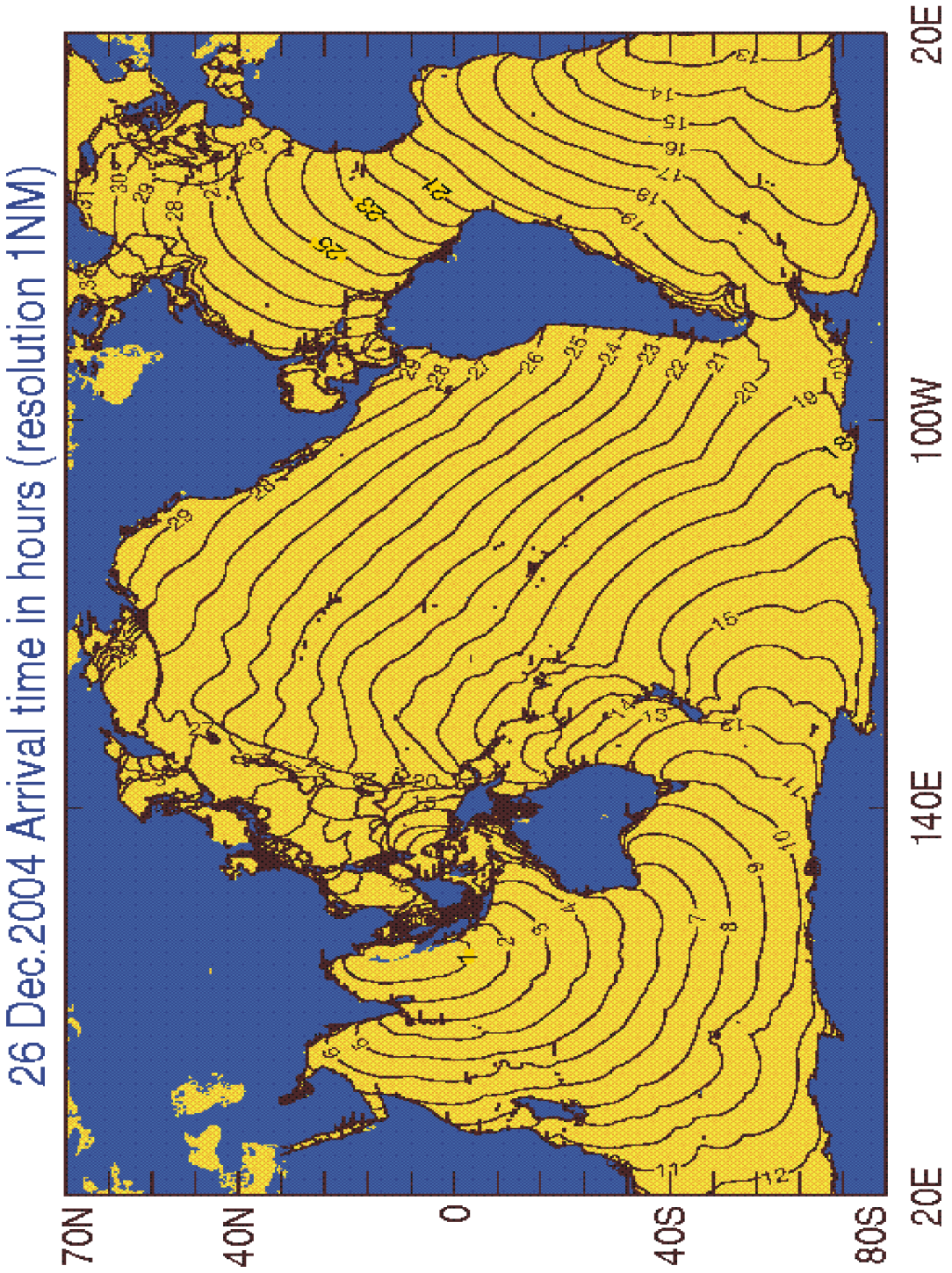

Figure 8. Travel time (in hours) for the tsunami of 0.1cm amplitude.

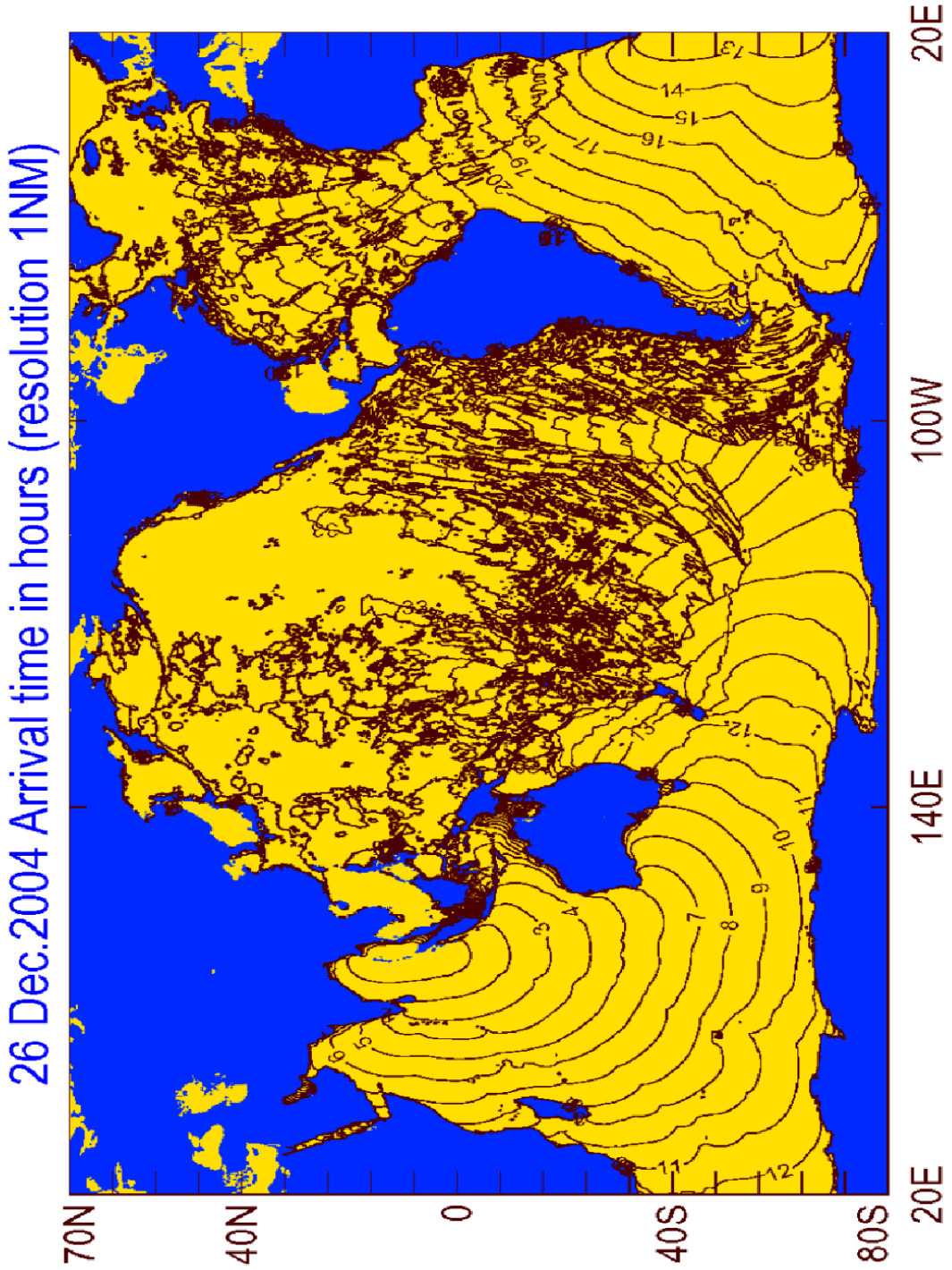

Figure 9. Travel time (in hours) for the tsunami of 0.5cm amplitude.

We were able to construct isolines in the regions of larger amplitudes, i.e. in Indian Ocean, in South Pacific (especially along the South Pacific Ridge) and in South Atlantic. By checking results of computation at the coastal locations it is easy to see that the tsunami of 0.5cm amplitude arrived at every location in the Pacific Ocean. This wave did not arrived at western North America by refracting around New Zealand; it traveled closer to South America via energy ducts located over South Pacific ridges. This is quite a long travel time as compared to the travel time depicted in Fig. 8.

In Table 2., the observed arrival time is compared with the computed arrival time of 0.1cm and 5cm tsunami amplitude. The observations define travel times uniquely when amplitude of the signal is above the noise level. The mixed signal of meteorological and tsunami origin is difficult to differentiate. We took, somewhat arbitrarily, the amplitude of 5cm as a signal strong enough to be seen above the meteorological noise. As can be seen from Figs. 8 and 9 in many locations, and as close to the source as New Zealand, the first waves to arrive were quite small and they slowly increased in amplitude. For example, the observed arrival time for the Jackson Bay, NZ is 18h18min while according to the sea level computed at 0.1cm at this location the arrival time for the first wave was 12h30min.

Table 2. Observed and calculated travel time.

Station location	Travel time observed	Travel time for 0.1cm amplitude	Travel time for 5cm amplitude
Chennai, (80°.17E, 13°.04N	2h36min	2h18min	2h20min
Male, (73°.52E, 4°.18N	3h25min	3h12min	3h18min
Hanimadhoo, (73°.17E, 6°.77N)	3h41min	3h24min	3h30min
Diego Garcia, (72°.40E, 7°.28S)	3h55min	3h40min	3h40min
Hillarys, (115°.73E, 31°.82S)	6h41min	6h24min	6h36min
Salalah, (54°.00E, 16°.93N)	7h17min	7h6min	7h6min
Pt. La Rue, (55°.53E, 4°.57S)	7h25min	7h24min	7h24min
Lamu, (40°.90E, 2°.27S)	9h9min	8h30min	8h30min
Zanzibar, (39°.18E, 6°.15S)	9h49min	10h24min	10h36min
Portland, (141°.60E, 38°.33S)	10h39min	9h48min	10h18min
Richard's Bay, (32°.08E, 28°.80S)	11h13min	11h00min	11h12min
Port Elizabeth, (25°.63E, 33°.97S)	12h28min	12h00min	12h6min
Jackson Bay, (168°.62E, 43°.98S)	18h18min	12h30min	19h30min
Arraial de Cabo, (42°.02W, 22°.97S)	21h56min	20h54min	21h30min
Arica, (70°.21W, 18°.22S)	26h36min	26h6min	29h20min
Char. Amalie,(64°.55W, 18°.20N)	28h42min	27h45min	33h30min
San Diego, (117°.12W, 32°.45N)	31h25min	29h0min	35h30min
Halifax, (63°.59W, 44°.66N)	31h30min	30h6min	32h6min
Atl.City,(74°.25W, 39°.21N)	31h48min	30h45min	33h30min
Toffino, (125°.55W, 49°.09N)	32h1min	29h0min	38h30min
Adak, (176°.65W, 51°.87N)	35h	27h	40h

In the Pacific Ocean the stations located in the Northern Pacific show the large dif-

ferences between the calculated and observed travel time. This is caused either by small tsunami signal to noise ratio or by multiple paths between the source and gauge locations. In the latter, especially important is an interaction of the higher energy tsunami signals which travel slowly over the oceanic ridges and the lower energy signals which travel faster over the deep oceanic regions.

Acknowledgements. We wish to express our gratitude to Juan Horrillo, Institute of Marine Science, University of Alaska, Fairbanks for testing our model and offering suggestions on the model improvements.

References

Aki, K. and P. G. Richards. 1980. Quantitative Seismology Theory and Methods Volume 2, W.H. Freeman and Co., 557 pp.

Flather, R.A. and Heaps, N.S. 1975. Tidal computations for Morecambe Bay. *Geophys. J. Royal Astr. Soc.*, **42**, 489-517.

Gill A. E. 1982. *Atmosphere-Ocean Dynamics*, Academic Press, 662 pp.

Goring D. 2005. Sumatra Tsunami at New Zealand Ports and Harbours, http://www.mulgor.co.nz/SumatraTsunami/index.htm.

HRV - Harvard CMT Catalog (2005). Harvard Seismology: Centroid-Moment Tensor Project, posted at http://www.seismology.harvard.edu/CMTsearch.html.

Imamura F. 1996. Review of tsunami simulation with a finite difference method. In *Long-Wave Runup Models*, H.Yeah, P. Liu and C. Synolakis, Eds, World Scientific, 25–42.

Iwasaki, S.I. (2005). Posting of Thailand tide gage data to Tsunami Bulletin Board, also posted at http://www.navy.mi.th/hydro/tsunami.htm.

Ji, C. (2004). Preliminary Result of the 04/12/26 (Mw 9.0), OFF W COAST of Northern Sumatra Earthquake, posted at
http://www.gps.caltech.edu/%7Ejichen/Earthquake/2004/aceh/aceh.html.

Kowalik, Z. 2003. Basic Relations Between Tsunami Calculation and Their Physics - II , *Science of Tsunami Hazards*, v. 21, No. 3, 154-173

Kowalik, Z. and Murty, T.S. 1993a. *Numerical Modeling of Ocean Dynamics*, World Scientific, 481 pp.

Kowalik, Z. and Murty, T.S. 1993b. Numerical simulation of two-dimensional tsunami runup. *Marine Geodesy*, 16, 87–100.

Longuet-Higgins, M. S. 1969. On the transport of mass by time-varying ocean currents, *Deep-Sea Res.*, 16, 431–447.

Mader, C. L. 2004. *Numerical Modeling of Water Waves*, CRC Press, 274 pp.

Mei, C. C. 1989. *The Applied Dynamics of Ocean Surface Waves,* World Scientific, 740 pp.

Merrifield, M.A., Y.L. Firing, G. Brundrit, R. Farre, B. Kilonsky, W. Knight, L. Kong, C. Magori, P. Manurung, W. Mitchell, F. Shillington, E.M.S. Wijeratne, J. Jardin, S. Nakahara, F.-Y. Porter, and N. Turesky (2005). Tide Gauge Observations of the Indian Ocean Tsunami, December 26, 2004, manuscript submitted to *Geophysical Research Letters* Jan., 2005.

NIO - India National Institute of Oceanography (2005). 26 December 2004 Tsunami, posted at http://www.nio.org/jsp/tsunami.jsp.

NEIC - U.S. National Earthquake Information Center (2004). Magnitude 9.0 OFF THE WEST COAST OF NORTHERN SUMATRA Sunday, December 26, 2004 at 00:58:53 UTC Preliminary Earthquake Report, posted at
http://neic.usgs.gov/neis/bulletin/neic_slav_ts.html

Okada, Y. (1985). Surface deformation due to shear and tensile faults in a half-space, *Bulletin of the Seismological Society of America*, 75, 1135-1154.

Rabinovich, A.B. 2005. Web compilation of tsunami amplitudes and arrival times. http://www-sci.pac.dfo-mpo.gc.ca/osap/projects/tsunami/tsunamiasia_e.htm.

Reid, R.O. and R.O. Bodine. 1968. Numerical model for storm surges in Galveston Bay. *J. Waterway Harbour Div.*, 94(WWI), 33–57.
SOI - Survey of India (2005). Preliminary report of tsunami observations, posted at http://www.surveyofindia.gov.in/tsunami4.htm.

Stein, S. and Okal E. (2005). Ultra-long period seismic moment of the great December 26, 2004 Sumatra earthquake and implications for the slip process, posted at http://www.earth.northwestern.edu/people/seth/research/sumatra2.html.

Yagi, Y. (2005). Preliminary Results of Rupture Process for 2004 OFF COAST OF NORTHERN SUMATRA Giant Earthqauke (ver. 1), posted at
http://iisee.kenken.go.jp/staff/yagi/eq/Sumatra2004/Sumatra2004.html.

Science of Tsunami Hazards, Vol 23, No. 1 (2005) ISSN 8755-6839

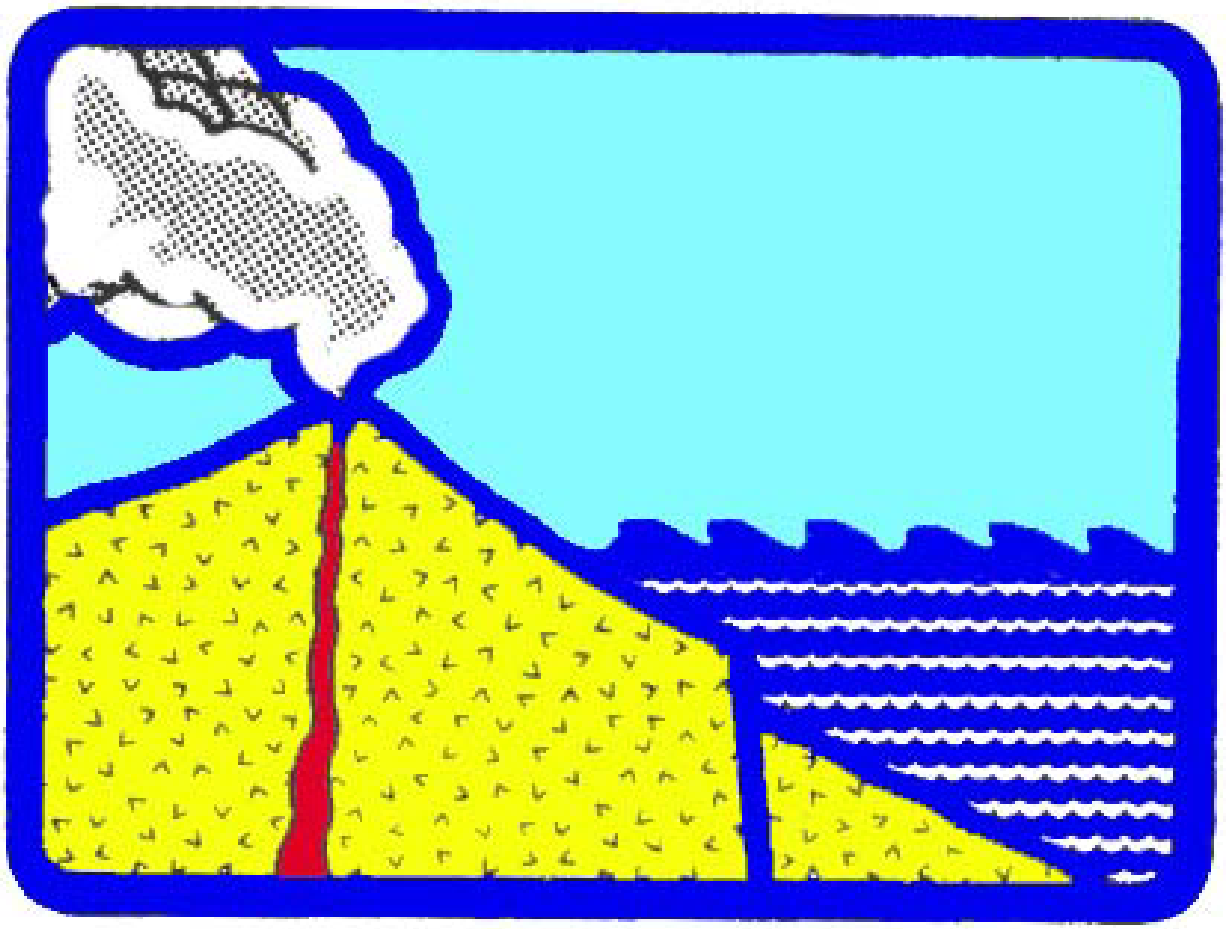

P. O. Box 1130,
Honolulu, HI 96807, USA

WWW.STHJOURNAL.ORG